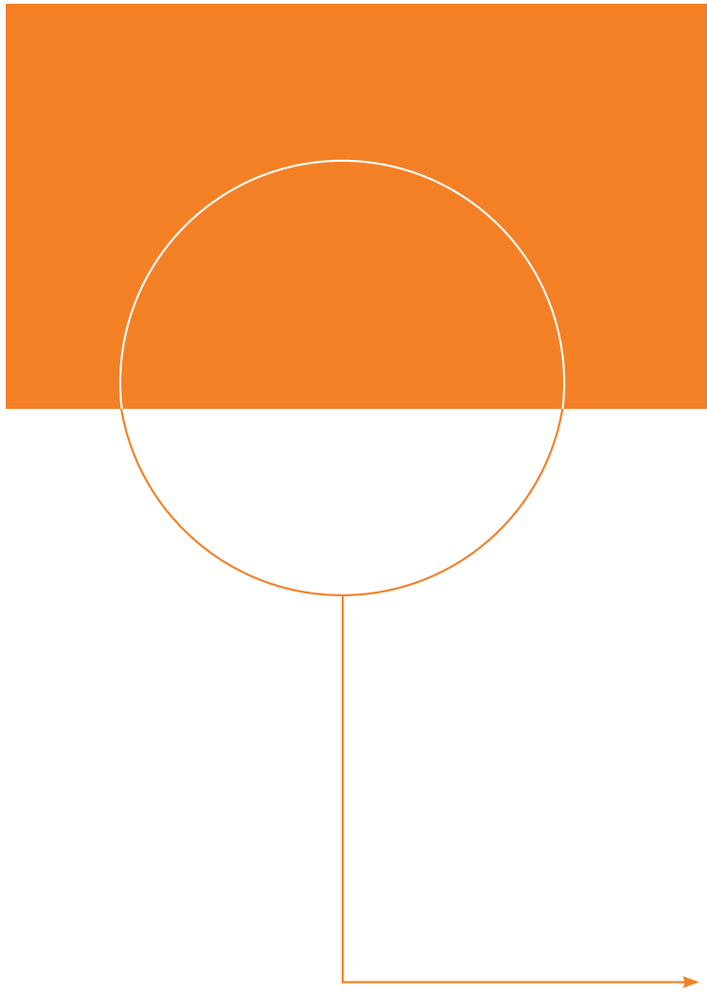

Master's thesis

2019

Xingyu Zhang

NTNU
Norwegian University of
Science and Technology
Faculty of Engineering
Department of Geoscience and Petroleum

Xingyu Zhang

Seismic signatures of vertically fractured media

June 2019

NTNU
Norwegian University of
Science and Technology

NTNU
Norwegian University of
Science and Technology

NTNU
Norwegian University of
Science and Technology

Seismic signatures of vertically fractured media

Xingyu Zhang

Applied Geophysics
Submission date: June 2019
Supervisor: Alexey Stovas

Norwegian University of Science and Technology
Department of Geoscience and Petroleum

Summary

Natural fractures are essential elements which can be commonly observed in reservoirs. The saying that "*All reservoirs should be considered fractured until proven otherwise.* (Narr et al., 2006)" is the best portrayal of its universality. The study of fracture systems is of great importance since it has been proven to have a strong impact on reservoir characteristics. The goal of this thesis is to figure out the relationship between seismic signatures and vertically fractured media.

In this thesis, first the effective VTI medium is obtained from well log data by using Backus averaging theory. Then, the effective ORT medium is constructed based on Schoenberg-Helbig model by embedding one vertical fracture set into VTI host medium. By comparing the anisotropy parameters, it is possible to detect one single fracture set between the host and effective media.

The combination of more vertical fracture sets (not parallel) and VTI background medium is supposed to provide effective MONO medium. However, two perpendicular fracture sets result in effective ORT medium. When summing up uniformly distributed vertical fractures within azimuthal angle $[-90^\circ, 90^\circ]$, the effective VTI medium is provided.

Numerical tests are performed to simulate more realistic fracture distributions by using Gaussian functions. The results show that it is very hard to distinguish between different fracture distributions through seismic signatures. However, for models in this study, certain geophysical methods can be applied to detect different distributions. This is very model-dependent. Therefore, in the future, more work should be done to obtain further correlation between seismic signatures and fracture systems.

Acknowledgements

I would like to thank my supervisor Prof. Alexey Stovas and his anisotropy group for their help with this thesis. My family needs thanks for helping me with trivial things which allowed me to focus. I also want to thank my cat Maolentin for releasing my stress and his very cute company. Most importantly, I would like to thank my husband Arne with love for everything. His love kept me sane through this thesis-writing period.

Table of Contents

List of Tables

List of Figures

Chapter 1

Introduction

1.1 Background

The role of seismic anisotropy has significantly increased over the past two decades due to progress in seismic acquisition and data processing (Tsvankin et al., 2010). It has contributed to increasing the success-rates in geophysical exploration and exploitation. Seismic anisotropy is defined to be *"The dependence of seismic velocities upon angle"* (Thomsen, 2014). Specifically, if the medium is anisotropic, the velocity of seismic waves vary with respect to different propagation directions. By contrast, heterogeneity is defined to be the dependence of physical properties upon spatial position (Tsvankin, 2012). In practice, it is very difficult to distinguish between heterogeneity and anisotropy. The concepts of these two properties are scale-dependent compared to seismic wavelength. The heterogeneity on a small scale can be transformed into homogeneous seismic anisotropy on a larger scale (Tsvankin, 2012).

There are various mechanics that can contribute to the anisotropy of sedimentary rocks (Thomsen, 1986).

- intrinsic anisotropy caused by the preferred orientation of anisotropic grains or the shapes of isotropic minerals;
- effective anisotropy due to fine isotropic or anisotropic layers on a small scale compared to seismic wavelength;
- Nonhydrostatic stresses;
- preferred orientation of fractures, microcracks or pores (fluids).

In reality, anisotropy is often the result of a certain combination of these factors (Tsvankin, 2012).

The hierarchy in seismic objects is going from crystals to minerals, then to rocks and finally to seismic layers with an increasing complexity. When it comes to the origin of anisotropy, it is considered to stem from crystals due to the crystal structure (Stovas and

Hao, 2015). Therefore, the minerals which consist of crystals naturally possess anisotropic features, which results in anisotropy in rocks (Thomsen, 2014). Therefore, upscalling methods are needed to develop anisotropy from crystals to seismic layers. In the hierarchy model, from minerals to seismic layers, they are both anisotropic and heterogeneous.

Upscaling theory is of great importance for geophysical research. By doing this procedure, heteorogenity is transformed into anisotropy. The number of model parameters are reduced as the effective medium is homogeneous. Only one set of parameters is required to describe the effective medium instead of one set for each layer.

1.2 Motivation

Well log data acquired over naturally fractured reservoirs often reveal the appearance of vertical fracture systems. The work of this thesis is to simulate different fracture distributions and to observe how they can affect seismic signatures. The goal is to analyze how the seismic anisotropy parameters of the medium can provide information to detect the characteristics of subsurface fracture networks.

1.3 Outline

This thesis consists of a summary, six chapters (including this introduction) and three appendices (Appendix A, Appendix B and Appendix C).

Chapter 1 provides the reader with a basic introduction to anisotropy. Then the motivation and chapter descriptions of this thesis are presented.

Chapter 2 presents more detailed information about anisotropy classes, including Isotropic (ISO), Transversely isotropic (TI), Orthorhombic (ORT) and Monoclinic (MONO) symmetries. The stiffness matrix, anisotropy parameters and the corresponding rock images of each anisotropy symmetry are introduced.

Seismic upscaling is the subject of Chapter 3. Upscaling theory is introduced and the application is stated. Additionally it brings up the concept of system matrix. Results from my Specialization project are presented and discussed here to support and provide more understanding of the theory.

Chapter 4 presents the workflow of the study. Each process from data quality control to the addition of vertical fractures is explained in detail and the corresponding results are elaborated upon. In this chapter, Backus theory is applied to obtain effective VTI media and Schoenberg-Muir model is used to build equivalent ORT media. The corresponding equations and matrices are listed.

Chapter 5 deals with fracture models. The fractures with various azimuthal angles are embedded by rotating the original ORT medium. The results are generalized and discussions are carried out on both analytical and numerical models.

Conclusions and continuations for future research are summarized in Chapter 6.

Appendix A presents the upscaling cases and model parameters taken from my Specialization project.

Appendix B provides the expressions of the elastic parameters in azimuthally rotated ORT media.

Appendix C gives the computation codes used in this study. Data quality control and upscaling process are done using Matlab R2018b while the fracture simulations are carried out using Wolfram Mathematica 10.0.

Chapter 2

Anisotropy symmetry systems

In this chapter, four anisotropy symmetries, which are of most importance in seismological applications, are described in detail. The definition, stiffness matrix and parameterization of each anisotropy symmetry are presented.

2.1 Isotropic medium

Isotropy is a common assumption applied in current exploration seismology theory. If the elastic properties in a medium do not change with direction, the medium is considered to be isotropic (ISO). In ISO medium, all planes are symmetry planes and it provides relatively simple computation procedures for seismic inversion and data processing. In reality, ISO medium appears in the following cases: intrinsic ISO without fractures; rocks that contain fractures distributed randomly and rocks that contain crystals or particles distributed randomly (Liang, 2009).

Figure 2.1: Quartzose sandstone from the Precambrian of Minnesota, USA (left) Source: https://www.flickr.com/photos/jsjgeology/23504564816; loose sedimentary sandstone (right) Source: https://www.flickr.com/photos/jsjgeology/1617030683 [With the permission of James St. John.]

To reveal the anisotropic properties of the medium, each anisotropic symmetry is characterized by a stiffness matrix with the number of independent parameters increasing for from high to low symmetries (Tsvankin, 2012). The stiffness matrix of isotropic medium is given by:

$$C_{iso} = \begin{bmatrix} \lambda+2\mu & \lambda & \lambda & 0 & 0 & 0 \\ \lambda & \lambda+2\mu & \lambda & 0 & 0 & 0 \\ \lambda & \lambda & \lambda+2\mu & 0 & 0 & 0 \\ 0 & 0 & 0 & \mu & 0 & 0 \\ 0 & 0 & 0 & 0 & \mu & 0 \\ 0 & 0 & 0 & 0 & 0 & \mu \end{bmatrix}. \tag{2.1}$$

It only contains two independent stiffness coefficients, here they are written in terms of Lame constants: λ and μ.

Based on the propagation and polarization directions, the body waves are categorized into three types: primary waves (P-waves) and two kinds of shear waves (S-waves). S-waves include Shear wave with vertical polarization (SV-wave) and Shear wave with horizontal polarization (SH-wave). In order to describe the isotropic medium, the velocities of P- and S-waves both independent on the propagation directions are defined:

$$V_p = \sqrt{\frac{\lambda+2\mu}{\rho}}, \tag{2.2}$$

$$V_s = \sqrt{\frac{\mu}{\rho}}.$$

2.2 Transversely isotropic medium

Although isotropy is a highly used model in exploration seismology theory, the fact that anisotropy widely exists in subsurface medium can not be denied (Xu, 2018). Therefore,

in seismic data processing, especially for the procedures highly sensitive to the accuracy of the velocity field, the anisotropic models are introduced to overcome the limitation and inadequacy of the ISO models.

The most common anisotropic model used in seismic analysis is transverse isotropy (TI). TI medium is defined to be that the elastic properties do not change in any directions perpendicular to the symmetry axis. Shale formation is considered to have intrinsic TI symmetry. Most shale formations are horizontally layered, yielding a transversely isotropic medium with a vertical symmetry axis (VTI). The periodic thin layering on a small scale compared to seismic wavelength also behaves as VTI symmetry (Tsvankin, 2012) (Figure 2.2).

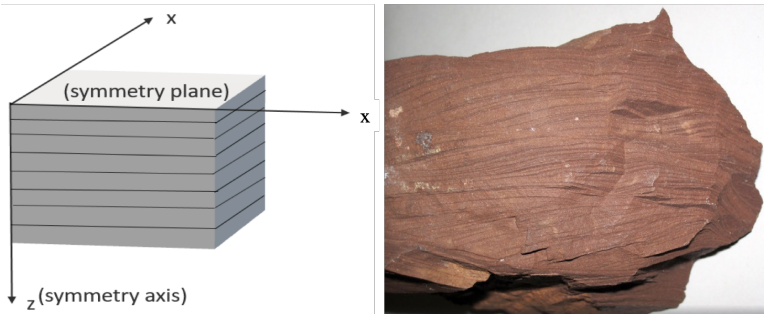

Figure 2.2: VTI model with symmetry planes and symmetry axis (left); Sandstone redbed samplle from the Triassic of Connecticut, USA (right) Source: https://www.flickr.com/photos/jsjgeology/41158229254. [With the permission of James St. John.]

The stiffness matrix of VTI medium with five independent parameters is given by:

$$C_{vti} = \begin{bmatrix} C_{11} & C_{11}-2c_{66} & C_{13} & 0 & 0 & 0 \\ C_{11}-2c_{66} & C_{11} & C_{13} & 0 & 0 & 0 \\ C_{13} & C_{13} & C_{33} & 0 & 0 & 0 \\ 0 & 0 & 0 & C_{44} & 0 & 0 \\ 0 & 0 & 0 & 0 & C_{44} & 0 \\ 0 & 0 & 0 & 0 & 0 & C_{66} \end{bmatrix}. \tag{2.3}$$

Although the stiffness matrix is convenient for forward modeling algorithms, Thomsen (Thomsen, 1986) introduced another notation for anisotropic parameterization of VTI medium which is convenient for reflection data processing (Tsvankin et al., 2010). With the new notation, the medium is described by five Thomsen parameters:

$$V_{p0} = \sqrt{\frac{C_{33}}{\rho}},$$

$$V_{s0} = \sqrt{\frac{C_{44}}{\rho}},$$

$$\epsilon = \frac{C_{11} - C_{33}}{2C_{33}}, \tag{2.4}$$

$$\delta = \frac{(C_{13} + C_{44})^2 - (C_{33} - C_{44})^2}{2C_{33}(C_{33} - C_{44})},$$

$$\gamma = \frac{C_{66} - C_{44}}{2C_{44}},$$

where V_{p0}, V_{s0} denote vertical P- and S-wave velocities, respectively. ρ is density, ϵ, δ and γ are dimensionless parameters which characterize the degree of anisotropy.

As shown in Equation 2.5 and 2.7, the physical meaning of ϵ and γ is that they govern the relation between horizontal propagation and vertical propagation of P and SH-waves, respectively. δ is defined by the second derivative of P-wave phase-velocity with vertical incidence (Equation 2.6). It also influences the SV-wave velocity (Stovas and Hao, 2015),

$$V_{px}^2 = V_{p0}^2(1 + 2\epsilon), \tag{2.5}$$

$$\frac{d^2V_p}{d\theta^2}|_{\theta=0} = 2V_{p0}\delta, \tag{2.6}$$

$$V_{shx}^2 = V_{s0}^2(1 + 2\gamma). \tag{2.7}$$

2.3 Orthorhombic medium

A more complicated anisotropy is the orthorhombic (ORT) model with three mutually orthogonal symmetry planes. It is common found in fractured reservoirs and is often used to describe the azimuthal dependency of elastic properties. The corresponding stiffness matrix with nine independent parameters is given by

$$C_{ort} = \begin{bmatrix} C_{11} & C_{12} & C_{13} & 0 & 0 & 0 \\ C_{12} & C_{22} & C_{23} & 0 & 0 & 0 \\ C_{13} & C_{23} & C_{33} & 0 & 0 & 0 \\ 0 & 0 & 0 & C_{44} & 0 & 0 \\ 0 & 0 & 0 & 0 & C_{55} & 0 \\ 0 & 0 & 0 & 0 & 0 & C_{66} \end{bmatrix}. \tag{2.8}$$

There are various reasons accounting for orthorhombic symmetry. The combination of VTI background medium with a set of vertical parallel fractures, the isotropic background medium with two sets of mutually orthogonal vertical fractures or the isotropic background medium with two non-orthogonal fracture sets having the same compliances, they all contribute to the behavior of orthorhombic anisotropy for seismic wave propagation (Kumar, 2013). The schematic diagram is shown in Figure 2.3.

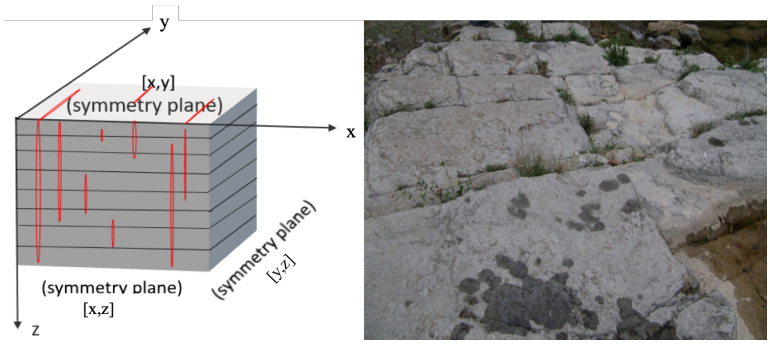

Figure 2.3: An ORT model caused by horizontal fine layers and vertical fractures (left); Geological outcrop of orthogonal joint (right). Source: http://wap. sciencenet.cn/blog.php?mobile=1 [With the permission of James St. John.]

The Thomsen-style paremeters were extended to orthorhombic medium by Tsvankin in (Tsvankin, 1997) in order to analyze the wave propagation:

$$
\begin{aligned}
V_{p0} &= \sqrt{\frac{C_{33}}{\rho}}, \\
V_{s0} &= \sqrt{\frac{C_{55}}{\rho}}, \\
\epsilon_2 &= \frac{C_{11} - C_{33}}{2C_{33}}, \\
\delta_2 &= \frac{(C_{13} + C_{55})^2 - (C_{33} - C_{55})^2}{2C_{33}(C_{33} - C_{55})}, \\
\gamma_2 &= \frac{C_{66} - C_{44}}{2C_{44}}, \\
\epsilon_1 &= \frac{C_{22} - C_{33}}{2C_{33}}, \\
\delta_1 &= \frac{(C_{23} + C_{44})^2 - (C_{33} - C_{44})^2}{2C_{33}(C_{33} - C_{44})}, \\
\gamma_1 &= \frac{C_{66} - C_{55}}{2C_{55}}, \\
\delta_3 &= \frac{(C_{12} + C_{66})^2 - (C_{11} - C_{66})^2}{2C_{11}(C_{11} - C_{66})},
\end{aligned}
\tag{2.9}
$$

where V_{p0} denotes vertical P-wave velocity. V_{s0} denotes the vertical velocity of the faster S-wave polirized in x-direction. $\epsilon_2, \delta_2, \gamma_2$ are identical to Thomsen parameters ϵ, δ, γ in symmetry plane [X,Z]. $\epsilon_1, \delta_1, \gamma_1$ are defined in symmetry plane [Y,Z], δ_3 is defined in symmetry plane [X,Y], based on the coordinate system in Figure 2.3.

ϵ_2 controls the relation between P-wave velocities along x- and z-axes. ϵ_1 controls the relation between P-wave velocities along y- and z-axes. Likewise, γ_1 and γ_2 have similar meaning as ϵ_1 and ϵ_2 but only for SH-wave. δ_2 is responsible for near-vertical P-wave velocity variation in [X,Z] plane while δ_1 is for plane [Y,Z]. δ_3 reveal the near-horizontal P-wave velocity variation in plane [X,Y] (Tsvankin, 1997).

Tsvankins notation for ORT medium preserves the attractive features of Thomsen parameters in describing the elastic properties of the symmetry-plane of P- and S-waves. It also provides a unified framework for treating ORT and TI models in parameter-estimation methods.

2.4 Monoclinic medium

Monoclinic (MONO) model is rather commonly being found in fractured reservoirs, but it is not widely used in seismic processing due to the large number (13) of independent parameters in the stiffness matrix:

$$C_{mon} = \begin{bmatrix} C_{11} & C_{12} & C_{13} & 0 & 0 & C_{16} \\ C_{12} & C_{22} & C_{23} & 0 & 0 & C_{26} \\ C_{13} & C_{23} & C_{33} & 0 & 0 & C_{36} \\ 0 & 0 & 0 & C_{44} & C_{45} & 0 \\ 0 & 0 & 0 & C_{45} & C_{55} & 0 \\ C_{16} & C_{26} & C_{36} & 0 & 0 & C_{66} \end{bmatrix}. \tag{2.10}$$

Multiple vertical fracture sets, possibly combined with horizontal fine layering (Figure 2.4), tilt fractures embedded in the ORT host medium and the ISO background medium with one set of micro-corrugated fractures, all produce an equivalent medium of MONO symmetry with a horizontal symmetry plane. In MONO symmetry, two vertical symmetry planes in ORT medium are gone.

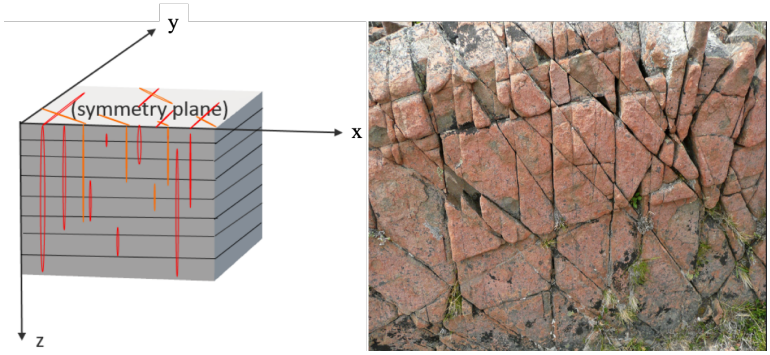

Figure 2.4: An MONO model of fractured reservoir (left); jointed rock near hosteria, South America(right). Source: https://www.flickr.com/photos/ jsjgeology/39608069664. [With the permission of James St. John]

The Thomsen-style parameterization of MONO medium was derived in (Grechka et al.,

2000):

$$
\begin{aligned}
V_{p0} &= \sqrt{\frac{C_{33}}{\rho}}, \\
V_{s0} &= \sqrt{\frac{C_{55}}{\rho}}, \\
\epsilon_2 &= \frac{C_{11} - C_{33}}{2C_{33}}, \\
\delta_2 &= \frac{(C_{13} + C_{55})^2 - (C_{33} - C_{55})^2}{2C_{33}(C_{33} - C_{55})}, \\
\gamma_2 &= \frac{C_{66} - C_{44}}{2C_{44}}, \\
\epsilon_1 &= \frac{C_{22} - C_{33}}{2C_{33}}, \\
\delta_1 &= \frac{(C_{23} + C_{44})^2 - (C_{33} - C_{44})^2}{2C_{33}(C_{33} - C_{44})}, \\
\gamma_1 &= \frac{C_{66} - C_{55}}{2C_{55}}, \\
\delta_3 &= \frac{(C_{12} + C_{66})^2 - (C_{11} - C_{66})^2}{2C_{11}(C_{11} - C_{66})}, \\
\zeta_1 &= \frac{C_{16}(C_{33} - C_{55}) - C_{36}(C_{13} - C_{55})}{C_{55}(C_{33} - C_{55})}, \\
\zeta_2 &= \frac{C_{26}(C_{33} - C_{44}) - C_{36}(C_{23} - C_{44})}{C_{44}(C_{33} - C_{44})}, \\
\zeta_3 &= \frac{C_{36}}{C_{33}}, \\
\zeta_4 &= \frac{C_{45}(C_{44} + C_{55})}{2C_{44}C_{55}},
\end{aligned}
\tag{2.11}
$$

where V_{p0}, V_{s0} denote vertical P- and S-wave velocities, respectively. The parameterization of MONO medium is similar to Tsvankin parameters mentioned in 2.3, but introduces four more parameters. $\epsilon_{1,2}, \delta_{1,2}$ and $\gamma_{1,2}$ are responsible for the pure-mode normal moveout (NMO) velocities along the x- and y- axes. δ_3 is not controlled by conventional-spread reflection traveltimes in a horizontal monoclinic layer. $\zeta_{1,2,3}$ cause the corresponding rotation of the S1, S2, and P-wave NMO ellipses with respect to the horizontal axes (Grechka et al., 2000). In addition, ζ_4 controls polarization of S1 and S2-waves in vertical direction. Note that there is shear-wave splitting phenomenon in anisotropic formation. When $C_{44} \neq C_{55}$, a vertical propagation field caused by a horizontal source oriented aslant with respect to the x- and y-axes will split into two different shear waves with distinct speeds and polarizations (Schoenberg and Helbig, 1997). It is common to consider the faster shear-wave to be S1-wave which polarizes along x-axis.

Chapter 3

Seismic upscaling

This Chapter mainly talks about the knowledge of upscaling theory and brings up the concept of system matrix of the medium. From the view of system matrix, the equations which are used for upscaling are presented. Partial numerical tests performed in specialization project (Zhang, 2018) are selected and presented here in order to demonstrate upscaling theory.

3.1 Upscaling theory

Seismic waves do not have enough resolution to detect the reflections of fine layers when the thickness of the sequence (length of averaging) is smaller than the seismic wavelength, the signals received can be regarded from a single averaged medium (Bandyopadhyay, 2009), as Figure 3.1 shows.

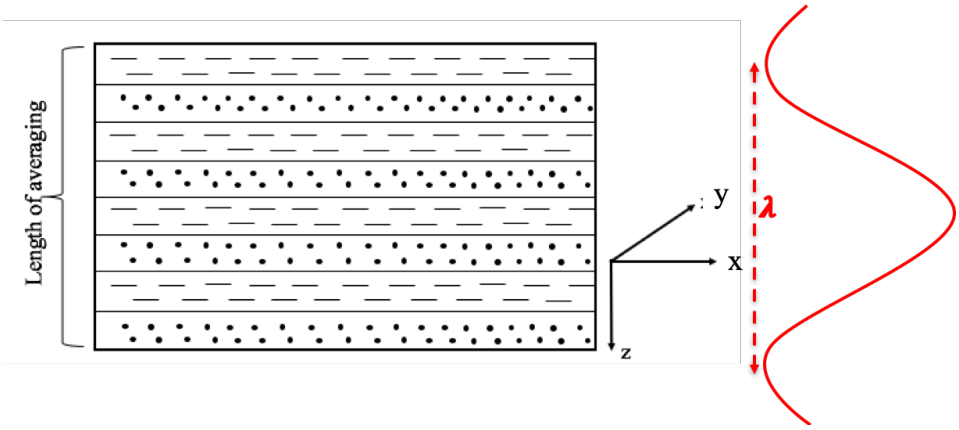

Figure 3.1: A stack of fine strata consisting of periodical VTI (shale) and ISO (sand) layers. λ is the wavelength. Practically the periodicity of layers is not required.

The equivalent medium is homogeneous and anisotropic. The symmetry of the equivalent medium is given by the lowest symmetry of the constituent layers (Zhang, 2018). The procedure of calculating the effective medium parameters is called upscaling. Backus averaging (Backus, 1962) is one of a specific method of upscaling which only deals with finely layered ISO or VTI constituents. However, more complicated anisotropies are present in the subsurface, especially fractured reservoirs. Schoenberg and Muir (Schoenberg and Muir, 1989) expanded the equations for arbitrary anisotropic constituent layers, which facilitates the research of reservoir characteristics. The assumptions which upscaling theory is based on are fine layers and stationarity (Schoenberg and Muir, 1989). Fine-layers means the length of averaging should not be more than one-third of seismic wavelength λ (Liner and Fei, 2006) and the individual layer thickness should be at least ten times smaller than λ (Mavko et al., 2009).

3.2 System matrix

3.2.1 MONO medium

Schoenberg and Muir (Schoenberg and Muir, 1989) theory can be used to compute the parameters for effective MONO media. For media with horizontal symmetry planes, the simplification can be done by averaging the corresponding system matrix (Fryer and Frazer, 1987).

First, the equation of motion in 1D medium is defined as:

$$\frac{d\mathbf{b}}{dz} = i\omega \mathbf{A}\mathbf{b}, \tag{3.1}$$

where $\mathbf{b}$ is the vector of stress-strain projections, ω is the frequency and $\mathbf{A}$ is the system matrix of the medium.

$$\mathbf{A} = \begin{bmatrix} 0 & \mathbf{M} \\ \mathbf{N} & 0 \end{bmatrix} \tag{3.2}$$

where $\mathbf{M}$ and $\mathbf{N}$ are symmetric matrices and defined by:

$$\mathbf{M} = \begin{bmatrix} -\rho & -p_1 & -p_2 \\ & -\frac{C_{44}}{(C_{44}C_{55}-C_{45}^2)} & \frac{C_{45}}{(C_{44}C_{55}-C_{45}^2)} \\ & & -\frac{C_{55}}{(C_{44}C_{55}-C_{45}^2)} \end{bmatrix} \tag{3.3}$$

$$\mathbf{N} = \begin{bmatrix} -\frac{1}{C_{33}} & -\frac{(p_1C_{13}+p_2C_{36})}{C_{33}} & -\frac{(p_1C_{36}+p_2C_{23})}{C_{33}} \\ & s_{11} & s_{12} \\ & & s_{22} \end{bmatrix} \tag{3.4}$$

with

$$s_{11} = (C_{11} - \frac{C_{11}^2}{C_{33}})p_1^2 + 2p_1p_2(C_{16} - \frac{C_{13}C_{36}}{C_{33}}) + (C_{66} - \frac{C_{36}^2}{C_{33}})p_2^2 - \rho,$$

$$s_{12} = (C_{16} - \frac{C_{13}C_{36}}{C_{33}})p_1^2 + (C_{12} + C_{66} - \frac{C_{13}C_{23}}{C_{33}}) - \frac{C_{36}^2}{C_{33}})p_2p_1 + (C_{26} - \frac{C_{23}C_{36}}{C_{33}})p_2^2,$$
$$s_{22} = (C_{66} - \frac{C_{36}^2}{C_{33}})p_1^2 + 2p_1p_2(C_{26} - \frac{C_{23}C_{36}}{C_{33}}) + (C_{22} - \frac{C_{23}^2}{C_{33}})p_2^2 - \rho, \tag{3.5}$$

note that p_1, p_2 are the horizontal slownesses in two orthogonal directions; C_{ij} denotes medium stiffness coefficients; ρ is medium density.

Based on Eq. 3.3, 3.4 and 3.5, the independent elements for monoclinic medium are obtained:

$$A_1 = \langle\frac{1}{C_{33}}\rangle, A_2 = \langle\frac{C_{13}}{C_{33}}\rangle, A_3 = \langle\frac{C_{36}}{C_{33}}\rangle, A_4 = \langle\frac{C_{23}}{C_{33}}\rangle,$$
$$A_5 = \langle\frac{C_{44}}{C_{44}C_{55} - C_{45}^2}\rangle, A_6 = \langle\frac{C_{55}}{C_{44}C_{55} - C_{45}^2}\rangle, A_7 = \langle\frac{C_{45}}{C_{44}C_{55} - C_{45}^2}\rangle,$$
$$A_8 = \langle C_{11} - \frac{C_{13}^2}{C_{33}}\rangle, A_9 = \langle C_{16} - \frac{C_{13}C_{36}}{C_{33}}\rangle, A_{10} = \langle C_{26} - \frac{C_{23}C_{36}}{C_{33}}\rangle, \tag{3.6}$$
$$A_{11} = \langle C_{66} - \frac{C_{36}^2}{C_{33}}\rangle, A_{12} = \langle C_{22} - \frac{C_{23}^2}{C_{33}}\rangle, A_{13} = \langle C_{12} + C_{66} - \frac{C_{13}C_{23}}{C_{33}} - \frac{C_{36}^2}{C_{33}}\rangle.$$

where $\langle\rangle$ denotes the averaged values. C_{ij} is the elastic parameters of each layer. In addition, the effective density can be calculated as,

$$\rho_e = \langle\rho\rangle. \tag{3.7}$$

By doing upscaling, the system matrix **A** of the medium is arithmetic averaged. In other words, all the independent elements of matrix **A** are averaged.

After the averaging properties listed in Eq.3.6 are obtained, the symmetric stiffness matrix of the effective monoclinic medium can be computed as follows:

$$\widetilde{\mathbf{C}} = \begin{bmatrix} \frac{A_2^2+A_1A_8}{A_1} & \frac{A_1(A_{13}-A_{11})+A_2A_4}{A_1} & \frac{A_2}{A_1} & 0 & 0 & \frac{A_2A_3+A_1A_9}{A_1} \\ & \frac{A_4^2+A_1A_{12}}{A_1} & \frac{A_4}{A_1} & 0 & 0 & \frac{A_4A_3+A_1A_{10}}{A_1} \\ & & \frac{1}{A_1} & 0 & 0 & \frac{A_3}{A_1} \\ & & & \frac{A_5}{A_5A_6-A_7^2} & \frac{A_7}{A_5A_6-A_7^2} & 0 \\ & & & & \frac{A_6}{A_5A_6-A_7^2} & 0 \\ & & & & & \frac{A_3^2+A_1A_{11}}{A_1} \end{bmatrix}. \tag{3.8}$$

Upscaling results: MONO+MONO

The model is composed of a stack of a repeating sequence of two different thin interbedding layers of MONO symmetry. α is introduced as volume fraction to represent the proportion of the second layer. When $\alpha = 0$, the model is equivalent to the first layer in composite while $\alpha = 1$ means the model is equivalent to the second layer. Model parameters can be found in Appendix A (Table 1). Figure 3.2 shows the result of how the anisotropy parameters change with respect to α.

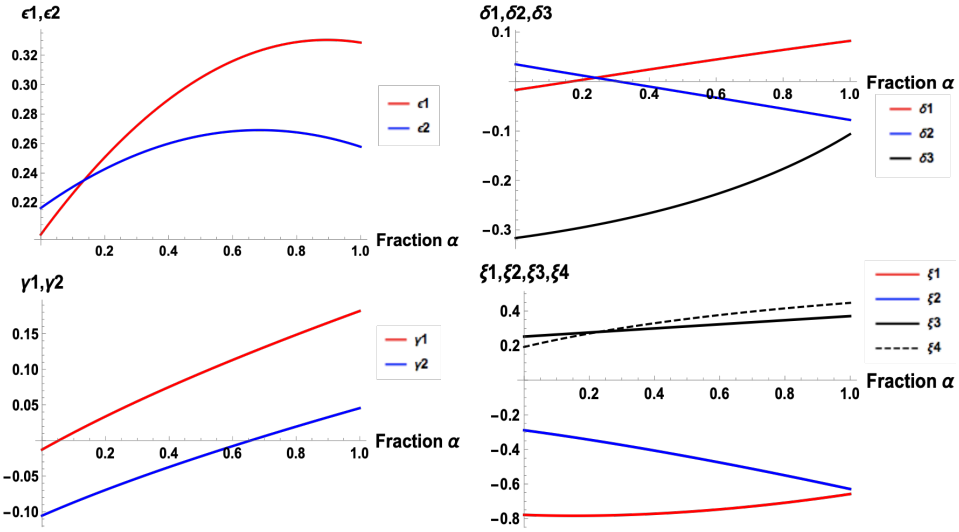

Figure 3.2: Anisotropy parameters of the effective MONO medium. (case: MONO+MONO)

With the increasing of α, ϵ_1 and ϵ_2 first increase then decrease, which results in a single peak for each curve. ϵ_1 is more affected by variation of α than ϵ_2. The maximum of ϵ_1 is 0.33 when α is 0.90 and the maximum of ϵ_2 is 0.27 when α is 0.66.

δ_1 and δ_3 are both increasing. δ_1 increases from negative to positive values and δ_3 is always negative over the entire range of α. δ_2 decreases from positive to negative values. δ_1 and δ_2 are close to linear while δ_3 is obviously nonlinear. δ_3 is more affected by variation of α compared to δ_1 and δ_2.

Both γ_1 and γ_2 are increasing nonlinearly from negative to positive values with increasing α and γ_1 is always larger than γ_2.

With the increasing of α, ζ_1 is increasing and close to the intersection with ζ_2. Meantime, ζ_3 and ζ_4 cross each other and increase gently. ζ_1 and ζ_2 are always negative; opposite of this, ζ_3 and ζ_4 are always positive.

Upscaling results: ORT+ORTϕ

This model is composed of a stack of a repeating sequence of two thin interbedding layers of ORT symmetry. The properties of these two layers are completely the same. But one of the constituents is azimuthally rotated with an angle ϕ with respect to x-axis. Since the parameters of rotated ORT medium are defined with ϕ, a table showing the parameter values can not be presented. However, the normal ORT medium parameters and the expressions of the parameters in the rotated ORT medium are shown in Appendix B.

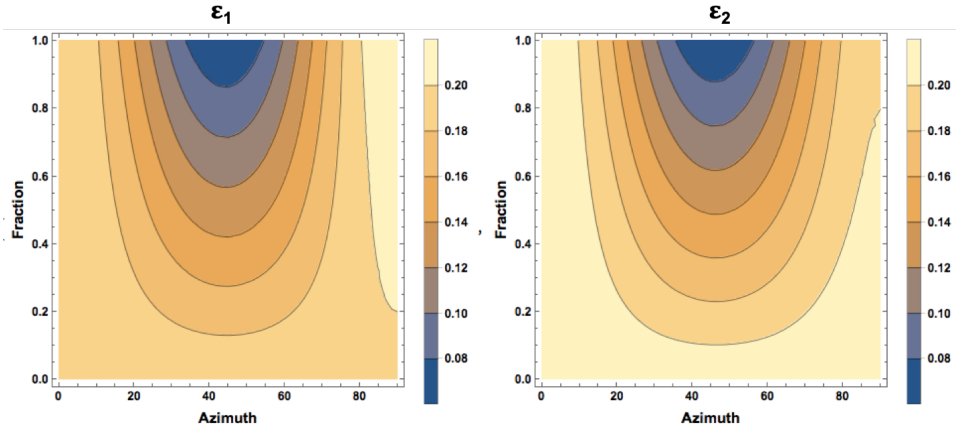

Figure 3.3: Anisotropy parameter ϵ of the effective MONO medium. (case: ORT+ORTϕ)

In Figure 3.3, ϵ_1 and ϵ_2 show a nearly symmetric trend about ϕ is 45 degrees and show a decreasing trend with increasing α. The minimum values of ϵ_1 and ϵ_2 are both 0.08 at (ϕ = 45 degrees, α = 1.0).

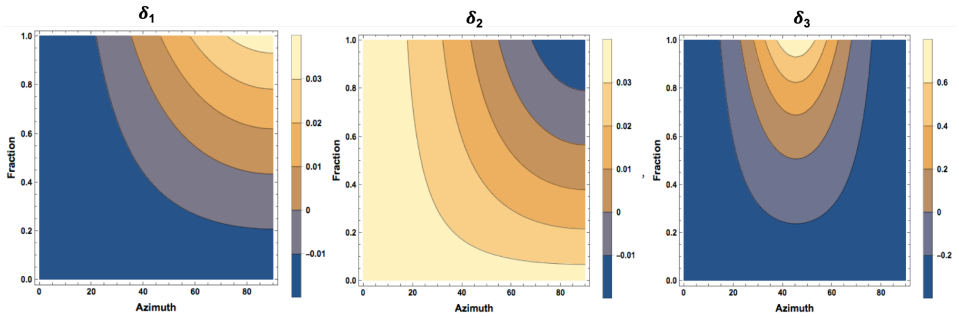

Figure 3.4: Anisotropy parameter δ of the effective MONO medium. (case: ORT+ORTϕ)

Figure 3.4 shows that δ_1 increases with respect to ϕ and α. The maximum value is 0.03 at (ϕ = 90 degrees, α = 1.0). δ_2 decreases with respect to ϕ and α. The minimum value is -0.01 at (ϕ = 90 degrees, α = 1.0). δ_3 shows a nearly symmetric trend about ϕ is 45 degrees and shows an increasing trend with α. The maximum value is about 0.6 around (ϕ = 45 degrees, α = 1.0)

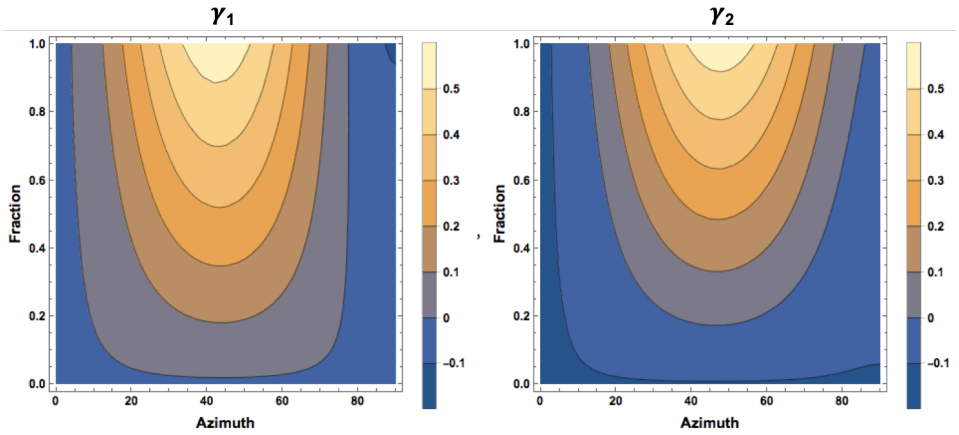

Figure 3.5: Anisotropy parameter γ of the effective MONO medium. (case: ORT+ORTϕ)

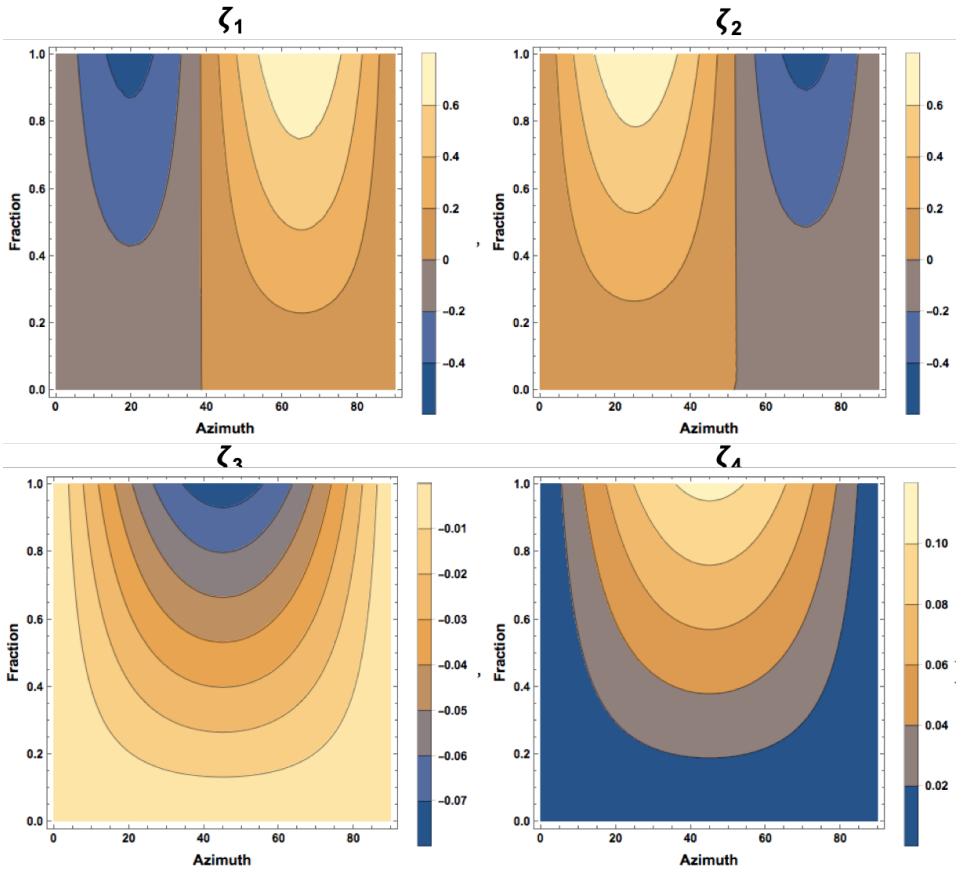

Figure 3.6: Anisotropy parameter ζ of the effective MONO medium. (case: ORT+ORTϕ)

From Figure 3.5, γ_1 and γ_2 are similar to ϵ_1 and ϵ_2 but with a completely opposite trend. γ_1 is approximately symmetric about ϕ is 42 degrees and shows an increasing trend with α. The maximum value is 0.5 at(ϕ = 42 degrees, α = 1.0). γ_2 has a approximately similar trend with γ_1. The maximum value is 0.5 at (ϕ = 47 degrees, α = 1.0).

In Figure 3.6, ζ_1 and ζ_2 show an interesting phenomenon. When ϕ is equal to 39 degrees, ζ_1 is 0 regardless of α. ζ_1 shows negative when ϕ is smaller than 39 degree and positive when ϕ is larger than 39 degrees. Likewise, when ϕ is equal to 52 degrees, ζ_2 is 0 regardless of α. ζ_2 shows positive when ϕ is smaller than 52 degrees and negative when ϕ is larger than 52 degrees. ζ_3 is nearly symmetric about ϕ is 45 degrees and shows a decreasing trend with increasing α. The minimum value is -0.07 at (ϕ = 45 degrees, α = 1.0). ζ_4 shows an opposite trend with ζ_3. The maximum value is 0.1 at (ϕ = 45 degrees, α = 1.0).

3.2.2 ORT medium

For the ORT case, C_{16}=0, C_{26}=0, C_{36}=0, C_{45}=0 are substituted into Eq. (3.3), (3.4) and (3.5). Therefore, the averaging properties are:

$$
\begin{aligned}
A_1 = \langle \frac{1}{C_{33}} \rangle, A_2 = \langle \frac{C_{13}}{C_{33}} \rangle, A_3 = \langle \frac{C_{23}}{C_{33}} \rangle, A_4 = \langle \frac{1}{C_{44}} \rangle, \\
A_5 = \langle \frac{1}{C_{55}} \rangle, A_6 = \langle C_{66} \rangle, A_7 = \langle C_{11} - \frac{C_{13}^2}{C_{33}} \rangle, \\
A_8 = \langle C_{22} - \frac{C_{23}^2}{C_{33}} \rangle, A_9 = \langle C_{12} + C_{66} - \frac{C_{13}C_{23}}{C_{33}} \rangle.
\end{aligned}
\tag{3.9}
$$

where $\langle\rangle$ denotes the averaged values. C_{ij} are the elastic parameters of each layer. In addition, the effective density can be calculated as:

$$
\rho_e = \langle \rho \rangle. \tag{3.10}
$$

Thus the symmetric stiffness matrix of the effective ORT medium is obtained:

$$
\widetilde{\mathbf{C}} = \begin{bmatrix}
\frac{A_2^2 + A_1 A_7}{A_1} & A_9 - A_6 + \frac{A_2 A_3}{A_1} & \frac{A_2}{A_1} & 0 & 0 & 0 \\
 & \frac{A_3^2 + A_1 A_8}{A_1} & \frac{A_3}{A_1} & 0 & 0 & 0 \\
 & & \frac{1}{A_1} & 0 & 0 & 0 \\
 & & & \frac{1}{A_4} & 0 & 0 \\
 & & & & \frac{1}{A_5} & 0 \\
 & & & & & A_6
\end{bmatrix}. \tag{3.11}
$$

Upscaling results: ORT+ORT

This model is composed of a stack of a repeating sequence of two different thin interbedding layers of ORT symmetry. Model parameters are presented in Appendix A (Table 2).

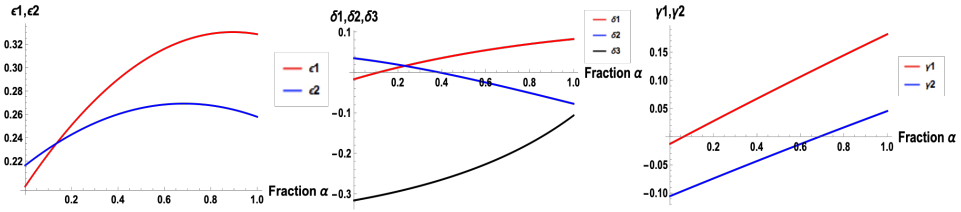

Figure 3.7: Anisotropy parameter of the effective ORT medium. (case: ORT+ORT)

It is obvious from the results that the effective medium is still of ORT symmetry. In the effective medium, the behavior of the Tsvankin parameters is similar to case 3.2.1 as discussed above. In this case, maximum of ϵ_1 is equal to 0.33 when α is 0.90 and maximum of ϵ_2 is equal to 0.27 when α is 0.66.

3.2.3 VTI medium

For the transversely isotropic (VTI) medium, Equations $C_{23} = C_{13}$, $C_{22} = C_{11}$, $C_{55} = C_{44}$, $C_{12} = C_{11} - 2C_{66}$ are substituted into Eq. (3.3), (3.4) and (3.5). Therefore, the averaging properties are obtained as:

$$A_1 = \langle \frac{1}{C_{33}} \rangle, A_2 = \langle \frac{C_{13}}{C_{33}} \rangle, A_3 = \langle \frac{1}{C_{55}} \rangle, A_4 = \langle C_{11} - \frac{C_{13}^2}{C_{33}} \rangle, A_5 = \langle C_{66} \rangle. \tag{3.12}$$

where $\langle\rangle$ denotes the averaged values. C_{ij} are the elastic parameters of each layer. In addition, the effective density can be calculated as:

$$\rho_e = \langle \rho \rangle. \tag{3.13}$$

Thus, the symmetric stiffness matrix of the effective VTI medium is shown as below:

$$\widetilde{\mathbf{C}} = \begin{bmatrix} \frac{A_2^2 + A_1 A_4}{A_1} & \frac{A_2^2 + A_1 A_4 - 2A_1 A_5}{A_1} & \frac{A_2}{A_1} & 0 & 0 & 0 \\ & \frac{A_2^2 + A_1 A_4}{A_1} & \frac{A_2}{A_1} & 0 & 0 & 0 \\ & & \frac{1}{A_1} & 0 & 0 & 0 \\ & & & \frac{1}{A_3} & 0 & 0 \\ & & & & \frac{1}{A_3} & 0 \\ & & & & & A_5 \end{bmatrix}. \tag{3.14}$$

Upscaling Results: ISO+ISO and VTI+VTI

First, the most basic model which is composed of a stack of periodical strata of two different ISO layers (Table 4) is tested. Then, both layers are VTI materials in the second model (Table 3). Model parameters are presented in Appendix A.

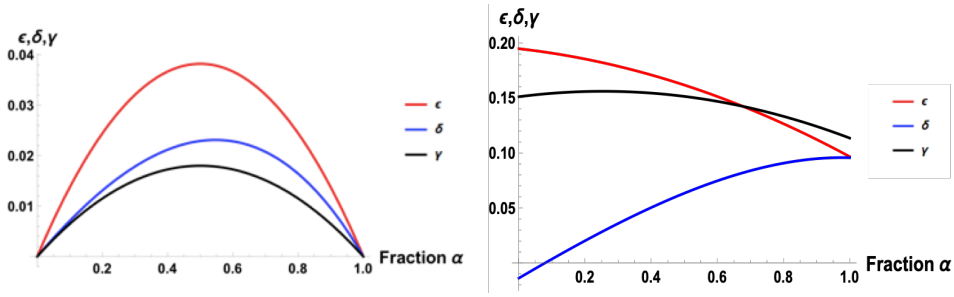

Figure 3.8: Anisotropy parameter of the effective VTI medium. (left case: ISO+ISO); (right case: VTI+VTI).

For the left case, Backus averaging of ISO layers results in the effective anisotropic (VTI) model. For increasing α, Thomsen parameters first increase then decrease. Note that at the two ends of α, all Thomsen parameters are equal to 0. That is because when α is 0, the model is equivalent to the first ISO medium in composite and when α is 1, the model is equivalent to the second ISO medium. In ISO medium, anisotropy parameters are always 0. Due to the feature of the figure, there are maximum values for ϵ, δ and γ. In this case, the maximum of ϵ is equal to 0.038 when α is 0.5. The maximum of γ is equal to 0.018 when α is also 0.5. The estimated maximum of δ is 0.023 when α is around 0.55 based on Figure 3.8. ϵ is the most affected by α of the three parameters while γ is the least.

For the case on the right, Thomsen parameters are no longer 0, which indicates that the effective medium is always VTI. With the increasing of α, ϵ and γ show a nonlinear decreasing tendency but they are always above 0. The maximum of γ is equal to 0.156 when α is 0.254. δ shows an nonlinear increasing tendency from negative value up to about 0.1.

Chapter 4

Data and methodology

The entire work of this thesis is presented in both Chapter 4 and 5. This chapter involves each step from the input data to the construction of orthorhombic (ORT) medium. A complete workflow is shown in methodology in order to give an overall impression about what has been done in this thesis.

4.1 Methodology

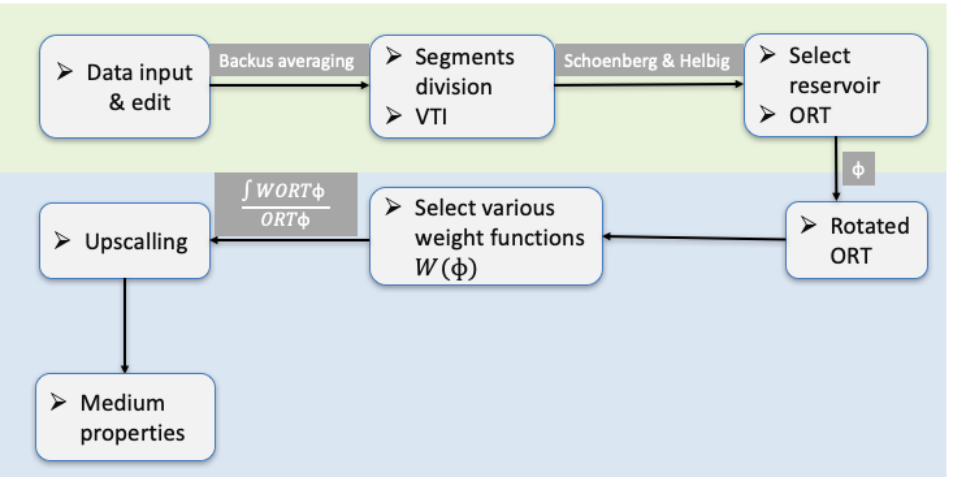

Figure 4.1: Workflow of the work in this thesis.

The workflow of this study is summarized in Figure 4.1. First, it is of great importance to edit the log data before all the calculations. Based on the information of Gamma-ray logs, the subsurface medium is divided into 7 blocks. With the help of Backus averaging,

each block is transformed into a homogeneous transversely isotropic (VTI) medium. One of the blocks which is considered to be the reservoir which composed of shale and sand laminations is chosen to carry out the following steps. The other 6 blocks are temporarily neglected. Afterwards, Schoenberg & Helbig (Schoenberg and Helbig, 1997) model is applied in order to build the equivalent ORT medium by adding vertical fractures. These steps are illustrated in green part of Figure 4.1.

All the blue part shows the work carried out in Chapter 5. The rotation of the ORT medium is done after the introduction of an azimuthal angle ϕ. Through selecting distinct intensity functions $W(\phi)$, fractures with different orientations are embedded. After applying upscaling, the stiffness matrix and anisotropy parameters of the effective medium can be computed.

4.2 Quality control

The study is performed on well log data acquired from the North Sea. There are 12165 samples in total with the depth ranging from 366.8m to 2220.6m. The interval of two neighbouring depths is 0.1524m. It contains the information of Gamma-ray, vertical P-wave velocity (v_{p0}), vertical S-wave velocity (v_{s0}), bulk density (ρ) and anisotropy parameters ϵ, δ and γ.

First of all, a quality control is done to the raw data. Due to some well logging factors, there are a lot of anomalies spread along the data with unrealistic negative values. Here two ways are used to fix the wrong points: in each column, if one point is bad, but its neighbouring data (in previous and following depths) are correct, it can be replaced by the averaged value of its neighbours; if several continuous data are all wrong, all the bad points will be removed. Figure 4.2 shows the full view of the log data used in this study (after removing unrealistic negative points).

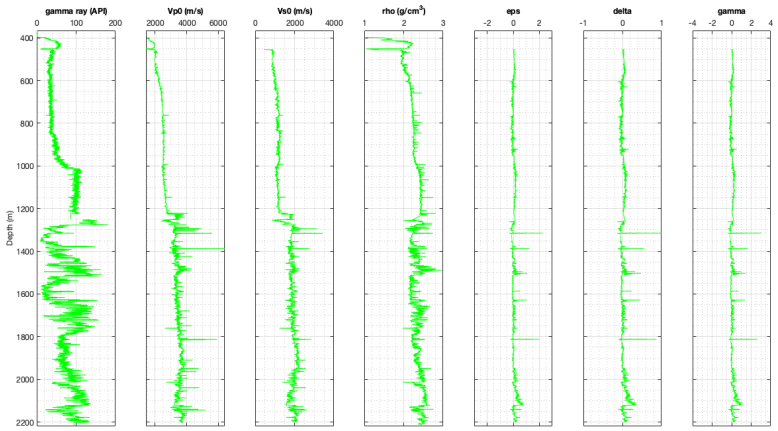

Figure 4.2: Well log data visualization after removing unrealistic negative points.

Through a general view of the data, the log condition is noted as following. For the Gamma-ray curve, there is an interruption at 1250-1252m depth due to the anomalies removing mentioned above. However, it does not affect the calculation in this study. For the P-wave velocity curve, data was not recorded until 400m depth while not until 452m depth for the S-wave and all three anisotropy parameters. From depth 452-455m, ϵ, δ and γ show 0 values, which indicates isotropic media. Last but not least, there are many spikes showing on the curves, which can probably affect the following steps, especially for v_{p0}, v_{s0}, ϵ, δ and γ. Note that most spikes appearing at the same depths (1315m, 1386m, 1586m, 1629m, 1812m) for all three anisotropy parameters.

Based on the feature of the data, for ϵ, δ and γ, a cutoff at 0.6 is set in order to remove all the anomalies above 0.6 using averaged value of neighbouring depths. For v_{p0}, v_{s0}, the cutoff are set at 4500m/s, 2500m/s, respectively. The result is shown below, note that Figure 4.3 is in the same scale as Figure 4.2 in order to be more suitable for comparison.

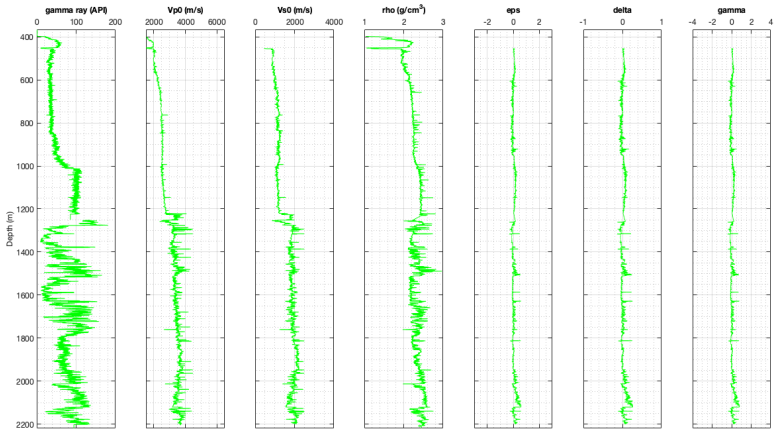

Figure 4.3: Well log data after removal of spikes.

4.3 Construction of the effective VTI medium

The Gamma-ray tools measure the natural gamma radiation in the formation and show a high value (80-300 API) in shale and a low value (30 API) in sandstone. Therefore, based on the Gamma-ray log, the data is divided into 7 blocks. (Table 4.1).

Figure 4.4 shows the block division. Block4 and Block6 are most likely sand-shale interbeds judging from the Gamma-ray log.

Table 4.1: Block depth intervals.

Blocks	Depth Interval
Block1	366–1016m
Block2	1016–1271m
Block3	1271–1433m
Block4	1433–1538m
Block5	1538–1650m
Block6	1650–1790m
Block7	1790–2220m

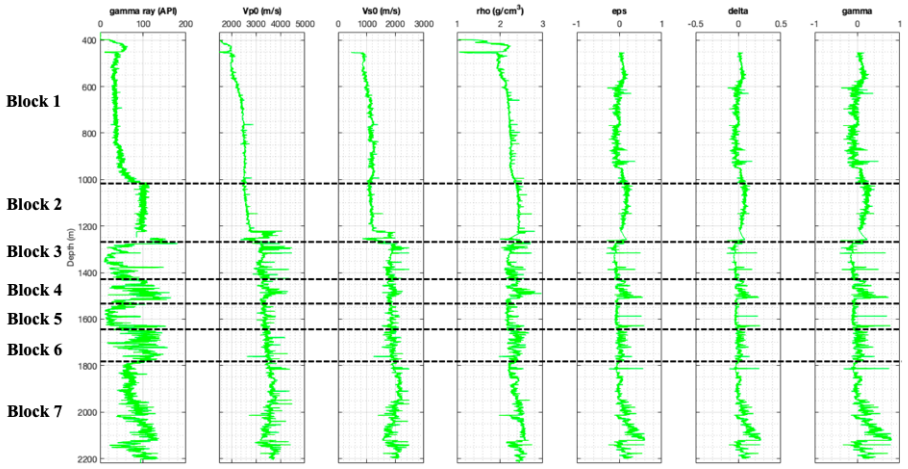

Figure 4.4: Block division.

Since all the values (v_{p0}, v_{s0}, ϵ, δ, γ) of each depth are provided, by using the inverse form of Eq.2.4 (as shown in Eq.4.1), all the stiffness coefficients for each depth can be obtained. Then, Eq. 3.12 is applied to calculate 5 independent elements of each depth.

$$
\begin{aligned}
C_{33} &= V_{p0}^2\rho, \\
C_{44} &= V_{s0}^2\rho, \\
C_{11} &= 2\epsilon C_{33} + C_{33}, \\
C_{13} &= \sqrt{(2\delta(C_{33}-C_{44}) + (C_{33}-C_{44})^2)} - C_{44}, \\
C_{66} &= 2\gamma C_{44} + C_{44},
\end{aligned}
\tag{4.1}
$$

where V_{p0}, V_{s0} denote vertical P- and S-wave velocities, respectively. ρ is layer density, ϵ, δ and γ are dimensionless anisotropy parameters which characterize the degree of anisotropy.

In the unit of each block, since each of the layers are weighted equally, arithmetic averaging equations (Eq.4.2) are applied to get the averaging properties $\widetilde{A_1}$ to $\widetilde{A_5}$ and ρ_e.

$$\widetilde{A_i} = \frac{1}{n}\sum_{j=1}^{n} A_{i,j}, i = 1, 2, ..5,$$

$$\rho_e = \frac{1}{n}\sum_{j=1}^{n} \rho_j, \tag{4.2}$$

where $\widetilde{A_i}$ represents the averaging properties of each block; n denotes the number of data in each block; $A_{i,j}$ is the independent element for each layer; j means the j-th layer. ρ_e is the effective density of each block, ρ_j means the density of each layer.

Using Eq.3.14 and Eq.2.4, stiffness coefficients (Table 4.2) and Thomsen parameters (Table 4.3) of the effective VTI medium are obtained. Initially, each depth is considered to be a homogeneous isotropic (ISO) or VTI layer. By doing Backus averaging, all the layers are divided into 7 effective homogeneous VTI media and the parameters (there are v_{p0}, v_{s0}, ρ, ϵ, δ, γ data for each depth) are reduced to 7 parameter sets, one set for each block.

Table 4.2: Stiffness coefficients after Backus averaging

	C11 (GPa)	C13 (GPa)	C33 (GPa)	C44 (GPa)	C66 (GPa)
Block1	11.756	6.217	10.824	2.405	2.595
Block2	22.776	11.453	17.680	3.488	5.065
Block3	20.157	7.784	23.682	7.504	6.035
Block4	29.958	11.406	26.670	7.892	9.159
Block5	22.924	8.961	25.091	7.767	6.878
Block6	30.265	11.963	28.533	8.384	9.095
Block7	36.452	13.000	30.541	9.257	1.168

Table 4.3: Thomsen parameters after Backus averaging

	v_{p0} (km/s)	v_{s0} (km/s)	ρ (g/cm^3)	ϵ	δ	γ
Block1	2.242	1.057	1.154	0.043	0.019	0.040
Block2	2.701	1.200	2.423	0.144	0.042	0.226
Block3	3.237	1.823	2.255	-0.075	-0.036	-0.099
Block4	3.374	1.835	2.343	0.062	0.020	0.080
Block5	3.365	1.872	2.216	-0.043	-0.023	-0.057
Block6	3.472	1.882	28.367	0.030	0.007	0.042
Block7	3.559	1.960	2.410	0.097	0.033	0.131

Figure 4.5 shows the result of Backus averaging:

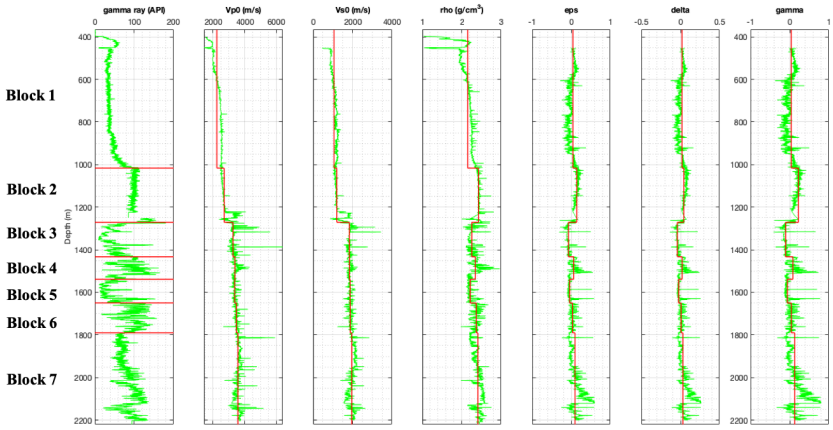

Figure 4.5: Backus averaging of vertical P-wave velocity, S-wave velocity, bulk density, anisotropy parameters ϵ, δ and γ. Red lines indicate the averaged values for each block. For Gamma-ray curve, red horizontal lines indicate the block division.

4.4 Construction of the effective ORT medium

Since Block4 is probably sand-shale interbed, it is common to be regarded as reservoir. Based on Backus theory introduced in Chapter 3, the equivalent medium after upscaling is transversely isotropic medium with a vertical symmetry axis (VTI). The stiffness tensor is

$$\mathbf{C}_b = \begin{bmatrix} 29.958 & 11.640 & 11.406 & 0 & 0 & 0 \\ & 29.958 & 11.406 & 0 & 0 & 0 \\ & & 26.670 & 0 & 0 & 0 \\ & & & 7.892 & 0 & 0 \\ & & & & 7.892 & 0 \\ & & & & & 9.159 \end{bmatrix}. \tag{4.3}$$

Here $\mathbf{C}_b$ means the tensor of the background medium.

Both horizontal fine layering and vertical fractures combined can contribute to a equivalent ORT medium under the long-wavelength limit (Schoenberg and Helbig, 1997). Therefore, referring to the Schoenberg-Helbig model, with the VTI medium as background, one vertical fracture set is embedded by introducing three fracture weakness elements. They are δ_N, δ_V, δ_H. δ_N is the strain that resulting from the normal fracture compliance; δ_V is the strain that resulting from the vertical tangential fracture compliance, and δ_H is the strain that is the result of the horizontal tangential fracture compliance. Schoenberg-Muir (Schoenberg and Muir, 1989) derived the expression showing the equivalent medium properties by adding the fracture compliance matrix to the background compliance matrix (Schoenberg and Helbig, 1997). The expression of stiffness matrix of effective medium is

given by:

$$\widetilde{\mathbf{C}_e} = \begin{bmatrix} \widetilde{\mathbf{c}_1} & 0 \\ 0 & \widetilde{\mathbf{c}_2} \end{bmatrix},$$

$$\widetilde{\mathbf{c}_1} = \begin{bmatrix} C_{11b}(1-\delta_N) & C_{12b}(1-\delta_N) & C_{13b}(1-\delta_N) \\ & C_{11b}(1-\delta_N \frac{C_{12b}^2}{C_{11b}^2}) & C_{13b}(1-\delta_N \frac{C_{12b}}{C_{11b}}) \\ & & C_{33b}(1-\delta_N \frac{C_{13b}^2}{C_{11b}C_{33b}}) \end{bmatrix},$$

$$\widetilde{\mathbf{c}_2} = \begin{bmatrix} C_{44b} & 0 & 0 \\ & C_{44b}(1-\delta_V) & 0 \\ & & C_{66b}(1-\delta_H) \end{bmatrix}. \tag{4.4}$$

The values of three fracture weaknesses are selected (Schoenberg and Helbig, 1997):

$$\delta_N = \frac{1}{10}, \delta_V = \frac{1}{5}, \delta_H = \frac{3}{11}. \tag{4.5}$$

Substituting Eq. 4.3 and 4.5 into expressions 4.4, the density-normalized symmetric stiffness matrix of the effective ORT medium is given by:

$$\widetilde{\mathbf{C}_e} = \begin{bmatrix} 26.987 & 10.500 & 10.265 & 0 & 0 & 0 \\ & 29.531 & 10.962 & 0 & 0 & 0 \\ & & 26.239 & 0 & 0 & 0 \\ & & & 7.892 & 0 & 0 \\ & & & & 6.314 & 0 \\ & & & & & 6.661 \end{bmatrix}. \tag{4.6}$$

The result will be used in Chapter 5 for further study.

By using Eq.2.9, the Tsvankin parameters of the effective ORT medium are computed. Here the anisotropy parameters of the background VTI medium and effective ORT medium are listed below:

Table 4.4: Parameter comparison of background and effective media.

	v_{p0}	$\mathbf{v_{s0}}$	ϵ_1	$\epsilon_\mathbf{2}$	δ_1	$\delta_\mathbf{2}$	$\delta_\mathbf{3}$	$\gamma_\mathbf{1}$	$\gamma_\mathbf{2}$
Model b	3.374	1.835	0.062	0.062	0.020	0.020	0	0.080	0.080
Model e	3.347	1.642	0.063	0.014	0.020	-0.117	-0.108	0.028	-0.078

Note that "Model b" and "Model e" denote the background VTI medium and the effective ORT medium, respectively. From Table 4.4, notice that both P and S-wave vertical velocities decrease when the vertical fracture set is added in the VTI background medium. As for other parameters, part of them are observed different between the media, as seen from ϵ_2, δ_2, δ_3, γ_1 and γ_2. It seems that by adding one set of vertical fractures, parameters in symmetry plane [X,Z] are more affected. It is probably because the fractures bring more effects to the perpendicular plane [X,Z] compared to the parallel plane. δ_3 appears in the equivalent ORT medium while in background VTI medium it is always 0. These observations provide a way of distinguishing between these two media and by extension detecting one set of vertical fractures.

Chapter 5

Effective media with fractures

The equivalent orthorhombic (ORT) medium obtained in Chapter 4 is rotated with an azimuthal angle varying from -90 degrees to 90 degrees. Through selecting diverse weight functions, different fracture orientations are simulated. The goal is to test and reveal how the fracture orientations affect the effective medium properties.

5.1 Analytical tests

In this section, four occasions of different fracture orientations are tested and the results are discussed.

5.1.1 ORT+ORTϕ

The model ORT+ORTϕ mentioned in case 3.2.1 in Chapter 3 is composed of a stack of a repeating sequence of two ORT interbedding layers with the same properties. One constituent is azimuthally rotated with an angle ϕ with respect to x-axis. Note that in this chapter, both the original ORT medium and the rotated ORT medium are in the same layer, as shown in Figure 5.1

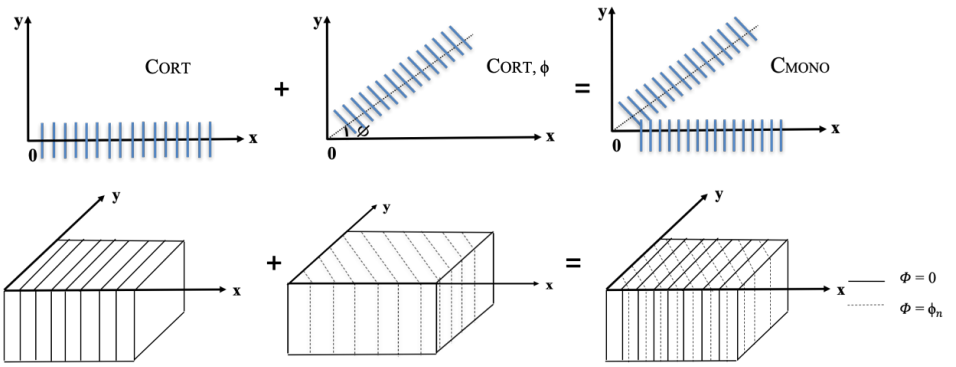

Figure 5.1: Schematic diagram of fracture orientations (above); Schematic diagram of fractured media (case: ORT+ORTϕ are in the same layer)(below).

In this case, the weight function is set as the Figure 5.2 shows. It only contains two sets of fractures: one is vertical whose normal is x-axis, the other is vertical with rotated azimuthal angle ϕ_n.

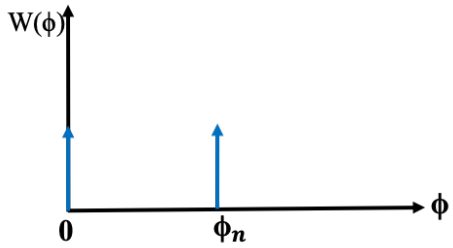

Figure 5.2: Weight function showing fracture orientations. The azimuthal angles of two fracture sets are 0 and ϕ_n, respectively.

Since the two fracture sets are in the same layer, the volume fraction of each medium is equal to $\frac{1}{2}$. Therefore, the averaging properties listed in Eq. 3.6 are changed into

$$\langle A_i \rangle = \frac{1}{2} A_{i1} + \frac{1}{2} A_{i2}, i = 1, 2, ...13, \tag{5.1}$$

where $\langle\rangle$ denotes the averaged values. A_{i1} represents the averaging properties of the medium embedded with a vertical fracture set; similarly, A_{i2} represents the averaging properties of the same fractured medium rotated with an azimuthal angle ϕ_n. The effective density ρ is defined to be

$$\rho_e = \langle \rho \rangle \tag{5.2}$$

In Schoenberg-Helbig (Schoenberg and Helbig, 1997) model, the medium density is not affected by fractures.

By using Eq.3.8 and 2.11, the results of ORT+ORTϕ are illustrated in Figure 5.3

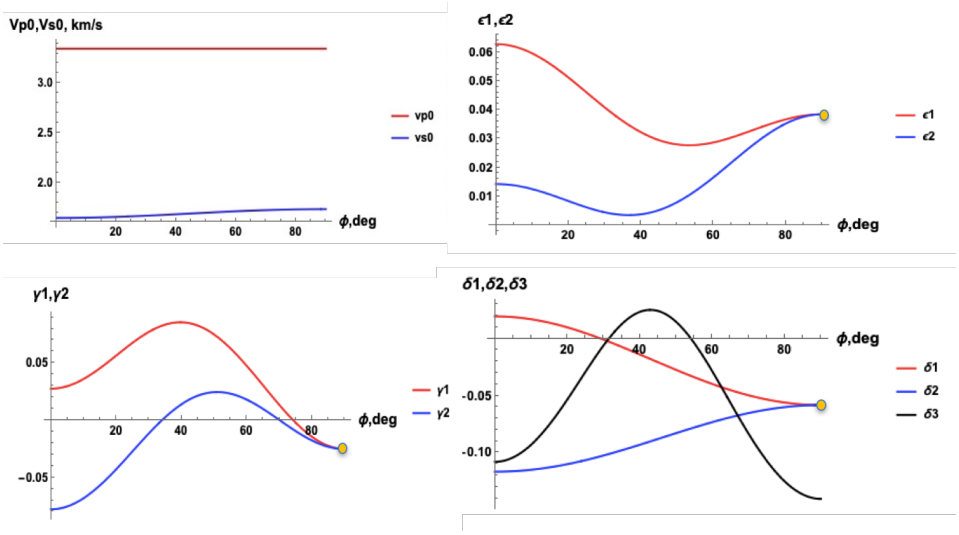

Anisotropy properties (vertical P- and S-wave velocities, Tsvankin parameters) of the effective MONO medium.

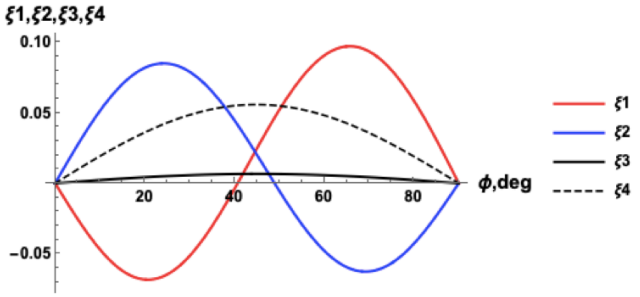

Figure 5.3: Anisotropy properties (four extra MONO parameters) of the effective MONO medium.

The vertical P-wave velocity (v_{p0}) is constant. That is due to the effective stiffness coefficient $\widetilde{C_{33}}$ does not depend on ϕ. The vertical S-wave velocity (v_{s0}) is slightly increasing with the increasing of angle ϕ.

ϵ_1 and ϵ_2 show a similar trend where they first decrease and then increase, which provides a minimum value. γ_1 and γ_2 similarly increase and then decrease, which can provide a maximum value. It shows an opposite trend compared to ϵ_1 and ϵ_2.

δ_1 and δ_2 are close to symmetric about around -0.06. δ_3 first increases and then decreases with a single peak. The behavior of δ_3 is quite different from δ_1 and δ_2.

ζ_1 and ζ_2 are close to symmetric about around $\phi = 45°$, they are highly affected by the changing of ϕ. ζ_4 is also obviously affected. It first increases and then decreases with a single peak at around $\phi = 45°$. However, ζ_3 shows similar tread as ζ_4 but only slightly changes with the increasing of ϕ, the peak is also around $\phi = 45°$.

Based on Figure 5.3, when $\phi_n = 0$, it represents there is only one set of vertical fractures, the equivalent medium is ORT; when $\phi_n \in (0, 90)$, it represents there is an azimuthal angle between two fracture sets, the equivalent medium is MONO.

Additionally, an interesting observation that should be noted is that $\phi_n = 90°$, ϵ_1 and ϵ_2 reach the same value. Likewise, γ_1 is equal to γ_2, δ_1 is equal to δ_2, indicated by the yellow dots. $\zeta_{1,2,3,4}$ are all 0 while δ_3 is not. More details will be analyzed in the following case.

5.1.2 ORT+ORT $\phi = 90°$

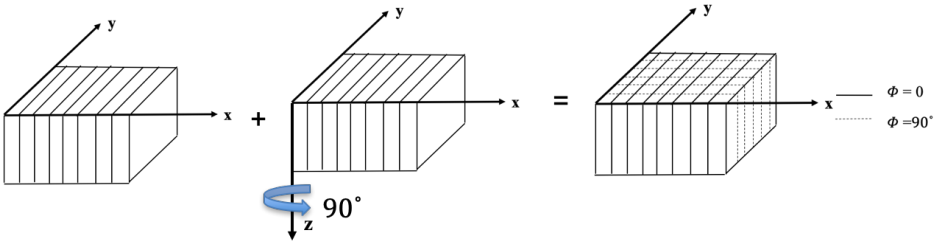

Figure 5.4: Schematic diagram of the fractured medium (case: ORT+ORT$_{90°}$ are in the same layer).

When $\phi_n = 90°$, there are two orthogonal vertical fracture sets, the symmetric effective stiffness matrix is obtained

$$\widetilde{\mathbf{C}} = \begin{bmatrix} C_{11} & C_{12} & C_{13} & 0 & 0 & 0 \\ & C_{11} & C_{13} & 0 & 0 & 0 \\ & & C_{33} & 0 & 0 & 0 \\ & & & C_{44} & 0 & 0 \\ & & & & C_{44} & 0 \\ & & & & & C_{66} \end{bmatrix} \tag{5.3}$$

It is a special case of ORT symmetry which contains six independent parameters. It indicates the two vertical symmetry planes are the same but the horizontal symmetry plane has azimuthal variation. Eq.5.4 show the expressions of each parameter:

$$\begin{aligned} \widetilde{C_{33}} &= C_{33}, \\ \widetilde{C_{11}} = \widetilde{C_{22}} &= -\frac{(C_{13} - C_{23})^2 - 2C_{33}(C_{11} + C_{22})}{4C_{33}}, \\ \widetilde{C_{13}} = \widetilde{C_{23}} &= \frac{C_{13} + C_{23}}{2}, \\ \widetilde{C_{44}} = \widetilde{C_{55}} &= \frac{2C_{44}C_{55}}{C_{44} + C_{55}}, \\ \widetilde{C_{12}} &= C_{12} + \frac{(C_{13} - C_{23})^2}{4C_{33}}, \end{aligned} \tag{5.4}$$

$$\widetilde{C_{66}} = C_{66},$$

where $\widetilde{C_{ij}}$ represents the elastic parameters of the effective ORT medium. C_{ij} represents the elastic parameters coming from the original ORT medium without rotation. From Eq. 5.4, we can see the horizontal propagation coefficients (C_{11}, C_{12}, C_{22}) are mainly governed by the difference between C_{13} and C_{23}. Effective $C_{13,23}$ correspond to the averaged properties of the two vertical symmetry planes. With the help of Eq. 5.4 and 2.11, the anisotropy parameters are given by

$$\epsilon_1 = \epsilon_2 = \frac{1}{2} - \frac{(C_{13} - C_{23})^2 - 2(C_{11} + C_{22})C_{33}}{8C_{33}^2},$$

$$\gamma_1 = \gamma_2 = \frac{1}{4}(-2 + \frac{C_{66}}{C_{44}} + \frac{C_{66}}{C_{55}}), \tag{5.5}$$

$$\delta_1 = \delta_2 = \frac{(C_{13} + C_{23} + 2C_{33})((C_{13} + C_{23} - 2C_{33})C_{44} + (C_{13} + C_{23} - 2C_{33} + 8C_{44})C_{55})}{8C_{33}(-2C_{44}C_{55} + C_{33}(C_{44} + C_{55}))},$$

$$\delta_3 = \frac{2(C_{11} + C_{22} + 2C_{12})C_{33}(-(C_{13} - C_{23})^2 + C_{33}(C_{11} + C_{22} - 2C_{12} - 4C_{66}))}{((C_{13} - C_{23})^2 - 2C_{33}(C_{11} + C_{22}))((C_{13} - C_{23})^2 - 2C_{33}(C_{11} + C_{22} - 2C_{66}))},$$

$\epsilon_{1,2}$ are governed by the difference between two vertical symmetry planes and P-wave propagation in both vertical and horizontal directions. $\gamma_{1,2}$ are governed by the S-wave propagation in both vertical and horizontal directions. δ_3 is related to the difference between two vertical symmetry planes and some horizontal parameters.

5.1.3 W=1 ($\phi : -\pi/2 \rightarrow \pi/2$)

In this case, the weight function is set as Figure 5.5 (left) shows. It is constant and equal to 1, which indicates the medium contains fractures with all azimuthal angles. When the x,y-axes turn clockwise the angle is negative while it is positive when turning counterclockwise as illustrated in Figure 5.5 (right).

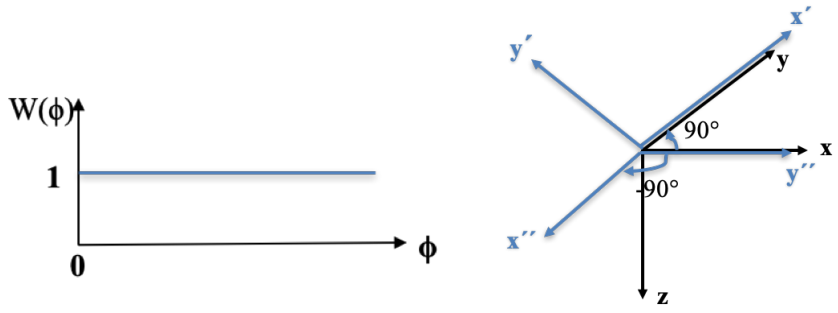

Figure 5.5: Weight function showing fracture orientations (left); Schematic diagram of rotated azimuthal angles from $-90°$ to $90°$(right).

Since the fractures oriented in all the directions and are equally dense, the integral Eq.5.6 is taken to get the averaging properties of the effective medium.

$$\langle WA_{\phi i}\rangle = \frac{\int_{-\frac{\pi}{2}}^{\frac{\pi}{2}} W(\phi)A_{\phi i}\mathrm{d}\phi}{\int_{-\frac{\pi}{2}}^{\frac{\pi}{2}} W(\phi)\mathrm{d}\phi}, i = 1, 2, ...13, \tag{5.6}$$

Since $W(\phi) = 1$, the integral turns into

$$\langle WA_{\phi i}\rangle = \frac{\int_{-\frac{\pi}{2}}^{\frac{\pi}{2}} A_{\phi i}\mathrm{d}\phi}{\pi}, i = 1, 2, ...13, \tag{5.7}$$

where W is the weight function, $A_{\phi i}$ is the averaging properties. It has 13 items in total as listed in Eq.3.6, the concrete expressions of $A_{\phi i}$ are listed in Appendix B. ϕ is the azimuthal angle of fractures. The effective density ρ is defined to be

$$\rho_e = \langle\rho\rangle \tag{5.8}$$

where $\langle\rangle$ denotes the averaged values. In Schoenberg-Muir model, the medium density is not affected by fractures.

By using Eq.3.8 and 2.11, the effective stiffness matrix is obtained

$$\widetilde{\mathbf{C}} = \begin{bmatrix} C_{11} & C_{11}-2C_{66} & C_{13} & 0 & 0 & 0 \\ & C_{11} & C_{13} & 0 & 0 & 0 \\ & & C_{33} & 0 & 0 & 0 \\ & & & C_{44} & 0 & 0 \\ & & & & C_{44} & 0 \\ & & & & & C_{66} \end{bmatrix} \tag{5.9}$$

The result shows the effective medium is VTI medium with 5 independent parameters. That is probably because between $-90°$ to $90°$, the fracture orientations are also symmetric. Considering the fracture intensity is the same, the averaged effect results in that there is no azimuthal variation. Eq.5.10 show the expressions of each parameter:

$$\begin{aligned} \widetilde{C_{33}} &= C_{33}, \\ \widetilde{C_{11}} = \widetilde{C_{22}} &= -\frac{(C_{13}-C_{23})^2 - C_{33}(3C_{11}+2C_{12}+3C_{22}+4C_{66})}{8C_{33}}, \\ \widetilde{C_{13}} = \widetilde{C_{23}} &= \frac{C_{13}+C_{23}}{2}, \\ \widetilde{C_{44}} = \widetilde{C_{55}} &= \frac{2C_{44}C_{55}}{C_{44}+C_{55}}, \\ \widetilde{C_{12}} &= \frac{(C_{13}-C_{23})^2 + C_{33}(C_{11}+6C_{12}+C_{22}-4C_{66})}{8C_{33}}, \\ \widetilde{C_{66}} &= -\frac{(C_{13}-C_{23})^2 - C_{33}(C_{11}-2C_{12}+C_{22}+4C_{66})}{8C_{33}}, \end{aligned} \tag{5.10}$$

where $\widetilde{C_{ij}}$ represents the elastic parameters of the effective ORT medium. C_{ij} represents the elastic parameters coming from the original ORT medium without rotation. Eq. 5.10 shows the expressions of $C_{44,55}$, $C_{13,23}$ are the same as the previous case 5.1.2. The horizontal propagation coefficients $C_{11,22}$ and C_{66} have the similar form, they are mainly governed by the difference between the C_{13} and C_{23}.

Considering Eq. 5.10 and 2.11, the velocities are

$$v_{p0} = \sqrt{\frac{C_{33}}{\rho_e}}, v_{s0} = \sqrt{\frac{2C_{55}C_{44}}{C_{44}+C_{55}\,\rho_e}}, \tag{5.11}$$

where v_{p0}, v_{s0} are vertical P-wave and S-wave velocity, respectively. ρ_e is density of the effective medium. C_{ij} denotes the elastic parameters of the ORT medium without rotation.

The anisotropy parameters are given by:

$$\epsilon_1 = \epsilon_2 = -\frac{(C_{13}-C_{23})^2 - C_{33}(3C_{11}+2C_{12}+3C_{22}-8C_{33}+4C_{66})}{16C_{33}^2},$$

$$\gamma_1 = \gamma_2 = \frac{(C_{44}+C_{55})(-\frac{2C_{44}C_{55}}{C_{44}+C_{55}} - \frac{(C_{13}-C_{23})^2-C_{33}(C_{11}-2C_{12}+C_{22}+4C_{66})}{8C_{33}})}{4C_{44}C_{55}}, \tag{5.12}$$

$$\delta_1 = \delta_2 = \frac{(C_{13}+C_{23}+2C_{33})((C_{13}+C_{23}-2C_{33})C_{44}+(C_{13}+C_{23}-2C_{33}+8C_{44})C_{55})}{8C_{33}(-2C_{44}C_{55}+C_{33}(C_{44}+C_{55}))},$$

The expressions of $\delta_{1,2}$ are the same as it in Case 5.1.2. $\epsilon_{1,2}$ are controlled by the difference between C_{13} and C_{23}. $\gamma_{1,2}$ are also controlled by the difference between C_{13} and C_{23}. In addition, they also depend on S-wave propagation coefficients C_{44} and C_{55}.

5.1.4 W=1 ($\phi : 0 \rightarrow \pi/2$)

In this case, the weight function is set as Figure 5.6 (left) shows. It is constant and equal to 1, which indicates the medium contains fractures with all azimuthal angles. On the right side of Figure 5.6, it explains when the x,y-axes turn counterclockwise the angle is positive.

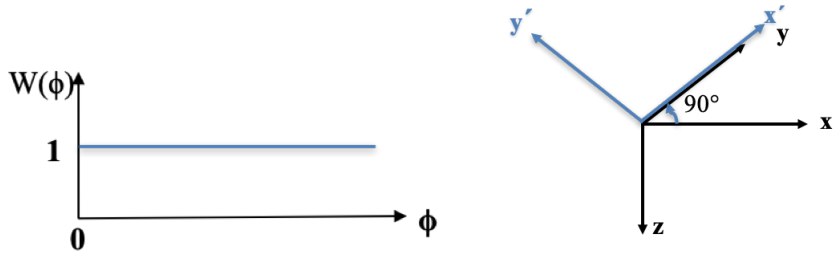

Figure 5.6: Weight function showing fracture orientations (left); Schematic diagram of rotated azimuthal angle from 0 to 90°(right).

Since the fractures oriented in all the directions and are equally dense, the integral (Eq.5.13) is taken to get the averaging properties of the effective medium.

$$\langle WA_{\phi i}\rangle = \frac{\int_0^{\frac{\pi}{2}} W(\phi)A_{\phi i}\mathrm{d}\phi}{\int_0^{\frac{\pi}{2}} W(\phi)\mathrm{d}\phi}, i = 1, 2, ...13, \tag{5.13}$$

Since $W(\phi) = 1$, the integral turns into

$$\langle WA_{\phi i}\rangle = \frac{2\int_0^{\frac{\pi}{2}} A_{\phi i}\mathrm{d}\phi}{\pi}, i = 1, 2, ...13, \tag{5.14}$$

where W is weight function, $A_{\phi i}$ is the averaging properties. It has 13 items in total as listed in Eq.3.6, the concrete expressions of $A_{\phi i}$ are listed in Appendix B. ϕ is the azimuthal angle of fractures. The effective density ρ is defined to be

$$\rho_e = \langle\rho\rangle \tag{5.15}$$

where $\langle\rangle$ denotes the averaged values. In Schoenberg-Muir model, the medium density is not affected by fractures.

By using Eq.3.8 and 2.11, the effective stiffness matrix is obtained:

$$\widetilde{\mathbf{C}} = \begin{bmatrix} C_{11} & C_{12} & C_{13} & 0 & 0 & C_{16} \\ & C_{11} & C_{13} & 0 & 0 & C_{16} \\ & & C_{33} & 0 & 0 & C_{36} \\ & & & C_{44} & C_{45} & 0 \\ & & & & C_{44} & 0 \\ & & & & & C_{66} \end{bmatrix}. \tag{5.16}$$

The result shows the effective medium is MONO medium with 8 independent parameters. Fractures in all the directions within 0 to 90° are summarized. Since the range is not symmetric, it can lead to some azimuthal variations. It matches the result which Eq. 5.16 shows. Eq.5.17 show the expressions of each parameter:

$$\begin{aligned}
\widetilde{C_{33}} &= C_{33}, \\
\widetilde{C_{11}} = \widetilde{C_{22}} &= -\frac{(C_{13}-C_{23})^2 - C_{33}(3C_{11}+2C_{12}+3C_{22}+4C_{66})}{8C_{33}}, \\
\widetilde{C_{13}} = \widetilde{C_{23}} &= \frac{C_{13}+C_{23}}{2}, \\
\widetilde{C_{44}} = \widetilde{C_{55}} &= \frac{2C_{44}C_{55}(C_{44}+C_{55})\pi^2}{-4(C_{44}-C_{55})^2 + (C_{44}+C_{55})^2\pi^2}, \\
\widetilde{C_{12}} = C_{11} - 2C_{66} &= \frac{(C_{13}-C_{23})^2 + C_{33}(C_{11}+6C_{12}+C_{22}-4C_{66})}{8C_{33}}, \\
\widetilde{C_{66}} &= -\frac{C_{33}(C_{11}-2C_{12}+C_{22}+4C_{66}) - \frac{(C_{13}-C_{23})^2(-8+\pi^2)}{\pi^2}}{8C_{33}},
\end{aligned} \tag{5.17}$$

$$\widetilde{C_{45}} = -\frac{4C_{44}C_{55}(C_{44}-C_{55})\pi}{-4(C_{44}-C_{55})^2+(C_{44}+C_{55})^2\pi^2},$$
$$\widetilde{C_{16}} = \widetilde{C_{26}} = \frac{-C_{11}+C_{22}}{2\pi},$$
$$\widetilde{C_{36}} = \frac{C_{23}-C_{13}}{\pi},$$

where $\widetilde{C_{ij}}$ represents the elastic parameters of the effective ORT medium. C_{ij} represents the elastic parameters coming from the original ORT medium without rotation. Eq. 5.17 shows the expressions of $C_{11,22}$, C_{12}, $C_{13,23}$ are the same as the previous case 5.1.3.

Considering Eq. 5.17 and 2.11, the velocities are

$$v_{p0} = \sqrt{\frac{C_{33}}{\rho_e}}, v_{s0} = \pi\sqrt{\frac{2C_{55}C_{44}(C_{44}+C_{55})}{(-4(C_{44}-C_{55})^2+(C_{55}+C_{44})^2\pi^2)\rho_e}}, \tag{5.18}$$

where v_{p0}, v_{s0} are vertical P-wave and S-wave velocity, respectively. ρ_e is the density of the effective medium. C_{ij} denotes the elastic parameters of the medium without rotation.

The anisotropy parameters are given by:

$$\epsilon_1 = \epsilon_2 = -\frac{(C_{13}-C_{23})^2 - C_{33}(3C_{11}+2C_{12}+3C_{22}-8C_{33}+4C_{66})}{16C_{33}^2},$$

$$\delta_3 = \frac{16HC_{33}(C_{13}-C_{23})^2}{((C_{13}-C_{23})^2 - C_{33}(3C_{11}+2C_{12}+3C_{22}+4C_{66}))(4(C_{13}-C_{23})^2 - C_{33}\pi^2 H)},$$
$$H = C_{11}+C_{22}+2C_{12},$$
$$\gamma_1 = \gamma_2, \delta_1 = \delta_2, \zeta_1 = \zeta_2, \tag{5.19}$$
$$\zeta_3 = \frac{C_{23}-C_{13}}{C_{33}\pi},$$
$$\zeta_4 = \frac{2(C_{44}-C_{55})}{(C_{44}+C_{55})\pi}.$$

The expressions of $\epsilon_{1,2}$ are the same as the previous case 5.1.3. $\gamma_{1,2}$ are too complicated to show in analytical form, similar for $\delta_{1,2}$ and $\zeta_{1,2}$. However, they are mainly controlled by the combination of S-wave propagation parameters C_{44} and C_{55}. δ_3 and ζ_3 are related to the difference between C_{13} and C_{23}. ζ_4 is governed by S-wave propagation parameters C_{44} and C_{55}.

5.2 Numerical tests

Subsurface formation is known to be more complicated. Usually the fractures are not distributed uniformly. Therefore, Gaussion function (Eq. 5.20) is applied to simulate more complex fracture orientations in subsurface media.

$$W(\phi) = \beta_1 \exp\left[-\alpha_1(\phi-\phi_{01})^2\right] + \beta_2 \exp\left[-\alpha_2(\phi-\phi_{02})^2\right], \tag{5.20}$$

where $W(\phi)$ is weight function. $\beta_{1,2}, \alpha_{1,2}, \phi_{01,02}$ are the function parameters. $\beta_{1,2}$ control the amplitude of the peak and $\alpha_{1,2}$ control the width. $\phi_{01,02}$ decide the location of the peak.

In this section, four different parameter sets are selected to emerge various fracture distributions caused by some possible crustal stress. The model parameters are shown in Table 5.1 corresponding to Figure 5.7

Table 5.1: Parameters of Gaussion functions

Models	β_1	β_2	α_1	α_2	ϕ_{01}	ϕ_{02}
W_1	100	50	$\frac{324}{5\pi^2}$	$\frac{216}{\pi^2}$	0	$\frac{\pi}{4}$
W_2	50	100	$\frac{216}{\pi^2}$	$\frac{324}{5\pi^2}$	0	$\frac{\pi}{4}$
W_3	80	80	$\frac{324}{5\pi^2}$	$\frac{216}{\pi^2}$	0	$\frac{\pi}{3}$
W_4	100	100	$\frac{648}{\pi^2}$	$\frac{2160}{\pi^2}$	0	$\frac{\pi}{6}$

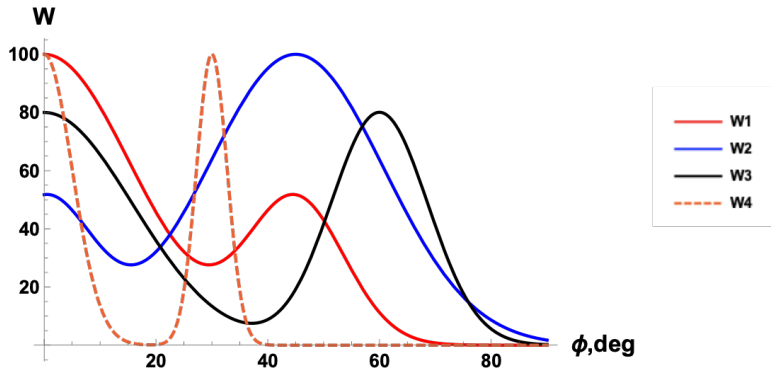

Figure 5.7: Gaussion distributions with four different parameter sets.

The integral is taken to average all independent elements

$$\langle WA_{\phi i}\rangle = \frac{\int_0^{\frac{\pi}{2}} W(\phi)A_{\phi i}\mathrm{d}\phi}{\int_0^{\frac{\pi}{2}} W(\phi)\mathrm{d}\phi}, i = 1, 2, ...13, \tag{5.21}$$

the effective density is

$$\rho_e = \langle\rho\rangle \tag{5.22}$$

where $\langle\rangle$ denotes the averaged values. In Schoenberg-Muir model, the medium density is not affected by fractures.

After all the averaging properties are calculated, by using Eq.3.8, the effective medium parameters are computed as.

The stiffness matrix for **model 1** is given by:

$$\widetilde{\mathbf{C}_1} = \begin{bmatrix} 25.506 & 11.547 & 10.421 & 0 & 0 & -0.050 \\ & 27.913 & 10.807 & 0 & 0 & 0.807 \\ & & 26.239 & 0 & 0 & 0.207 \\ & & & 7.509 & 0.468 & 0 \\ & & & & 6.637 & 0 \\ & & & & & 7.707 \end{bmatrix}, \tag{5.23}$$

The following are the stiffness matrix for **model 2,3** and **4**, respectively

$$\widetilde{\mathbf{C}_2} = \begin{bmatrix} 26.577 & 12.035 & 10.574 & 0 & 0 & 0.443 \\ & 26.871 & 10.654 & 0 & 0 & 0.558 \\ & & 26.239 & 0 & 0 & 0.274 \\ & & & 7.161 & 0.618 & 0 \\ & & & & 6.980 & 0 \\ & & & & & 8.195 \end{bmatrix}, \tag{5.24}$$

$$\widetilde{\mathbf{C}_3} = \begin{bmatrix} 26.990 & 11.565 & 10.558 & 0 & 0 & 0.498 \\ & 27.398 & 10.670 & 0 & 0 & 0.294 \\ & & 26.239 & 0 & 0 & 0.217 \\ & & & 7.177 & 0.488 & 0 \\ & & & & 6.926 & 0 \\ & & & & & 7.724 \end{bmatrix}, \tag{5.25}$$

$$\widetilde{\mathbf{C}_4} = \begin{bmatrix} 26.434 & 11.396 & 10.359 & 0 & 0 & -0.306 \\ & 28.292 & 10.868 & 0 & 0 & 0.964 \\ & & 26.239 & 0 & 0 & 0.180 \\ & & & 7.660 & 0.407 & 0 \\ & & & & 6.510 & 0 \\ & & & & & 7.557 \end{bmatrix}, \tag{5.26}$$

By using Eq.2.11, the anisotropy parameters are obtained:

Table 5.2: Tsvankin parameters of effective media

	v_{p0} km/s	v_{s0} km/s	ϵ_1	ϵ_2	δ_1	δ_2	δ_3	γ_1	γ_2
Original ORT	3.347	1.683	0.032	0.005	-0.016	-0.091	0.017	0.081	0.013
Model 1	3.347	1.683	0.032	0.005	-0.016	-0.091	0.017	0.081	0.013
Model 2	3.347	**1.726**	**0.012**	0.006	**-0.047**	-0.062	**0.073**	0.087	**0.072**
Model 3	3.347	1.719	0.022	**0.014**	-0.045	-0.066	0.001	**0.058**	0.038
Model 4	3.347	1.667	0.039	0.004	-0.002	**-0.101**	0.003	0.080	-0.007

Table 5.3: Four extra MONO parameters of effective media

	ζ_1	ζ_2	ζ_3	ζ_4
Original ORT	0	0	0	0
Model 1	-0.035	0.080	0.008	0.066
Model 2	0.028	0.042	**0.101**	**0.087**
Model 3	0.044	**0.123**	0.008	0.069
Model 4	**-0.071**	0.102	0.007	0.058

In Tables above, Original ORT represents the ORT medium without any azimuthal rotation. The results are showing that in all the models, v_{p0} is a constant regardless of model parameters. That is because v_{p0} is controlled by C_{33}, C_{33} is defined on z-axis and it is not affected by azimuthal rotation. Some of the other parameters are observed obviously different from the original medium, as seen from the bold numbers in the Tables above. These bold anisotropy parameters can help to distinguish between different fracture intensity and orientations.

Chapter 6

Conclusion

The main focus of this thesis is the seismic signatures of vertically fractured media. Upscaling theory and Schoenberg-Helbig model are the foundation throughout this study.

Effective ORT medium is constructed by combining fine layered background VTI medium and one vertical fracture set. By comparing the anisotropy parameters between the background and effective media, it is possible to detect the vertical fracture set in terms of calculated anisotropy parameters.

Then the ORT medium is rotated based on various weight functions. When there are more than one set of vertical fractures embedded, the effective medium appears to be MONO. However, there are two special cases. The effective medium parameters for special cases of the azimuthally rotated ORT medium are analytically derived, as seen in Eq. 5.4, 5.5 for the effective ORT medium and Eq.5.10-5.12 for the effective VTI medium.

The non-uniform distribution of fractures (Gaussian function) are introduced and the effective model parameters are numerically computed. From several examples, the conclusion can be drawn that it is very difficult to distinguish between the different fracture distributions. However, this is the model dependent problem. In particular, the distributions related to model 2 and 3, can be detected by using 3D non-hyperbolic semblance analysis and AVAZ method.

For the numerical tests, the values of the results are limited due to the model input. The continuation of this thesis is suggested to perform similar fracture simulations with Gaussian functions using variable-controlling approach to get more idea about how the fracture distributions affect model parameters.

Bibliography

Backus, G. E., 1962. Long-wave elastic anisotropy produced by horizontal layering. Journal of Geophysical Research 67 (11), 4427–4440.

Bandyopadhyay, K., 2009. Seismic anisotropy: Geological causes and its implications to reservoir geophysics. Stanford University.

Fryer, G. J., Frazer, L. N., 1987. Seismic waves in stratified anisotropic mediaii. elastodynamic eigensolutions for some anisotropic systems. Geophysical Journal International 91 (1), 73–101.

Grechka, V., Contreras, P., Tsvankin, I., 2000. Inversion of normal moveout for monoclinic media. Geophysical Prospecting 48 (3), 577–602.

Kumar, D., 2013. Applying backus averaging for deriving seismic anisotropy of a long-wavelength equivalent medium from well-log data. Journal of Geophysics and Engineering 10 (5), 055001.

Liang, K., 2009. The study on propagation feature and forward modeling of seismic wave in ti media. Ph.D. thesis, China University of Petroleum, Dongying, 17- 21.

Liner, C. L., Fei, T. W., 2006. Layer-induced seismic anisotropy from full-wave sonic logs: Theory, application, and validation. Geophysics 71 (6), D183–D190.

Mavko, G., Mukerji, T., Dvorkin, J., 2009. The rock physics handbook: Tools for seismic analysis of porous media. Cambridge university press.

Narr, W., Schechter, D., Thompson, L., 2006. Naturally fractured reservoir characterization: Spe.

Schoenberg, M., Helbig, K., 1997. Orthorhombic media: Modeling elastic wave behavior in a vertically fractured earth. Geophysics 62 (6), 1954–1974.

Schoenberg, M., Muir, F., 1989. A calculus for finely layered anisotropic media. Geophysics 54 (5), 581–589.

Stovas, A., Hao, Q., 2015. Seismic waves. Lecture notes.

Thomsen, L., 1986. Weak elastic anisotropy. Geophysics 51 (10), 1954–1966.

Thomsen, L., 2014. Understanding seismic anisotropy in exploration and exploitation. Society of Exploration Geophysicists.

Tsvankin, I., 1997. Anisotropic parameters and p-wave velocity for orthorhombic media. Geophysics 62 (4), 1292–1309.

Tsvankin, I., 2012. Seismic signatures and analysis of reflection data in anisotropic media. Society of Exploration Geophysicists.

Tsvankin, I., Gaiser, J., Grechka, V., Van Der Baan, M., Thomsen, L., 2010. Seismic anisotropy in exploration and reservoir characterization: An overview. Geophysics 75 (5), 75A15–75A29.

Xu, S., 2018. Seismic data processing in orthorhombic anisotropic media. Ph.D. thesis, Norwegian university of science and technology.

Zhang, X., 2018. Seismic signatures of fractured models. Project Report, Trondheim, Norwegian University of Science and Technology.

Appendix A: Parameters of effective medium

As presented in Chapter 3, the upscaling cases and model parameters shown below are from specialization project (Zhang, 2018).

A.1 Effective MONO medium

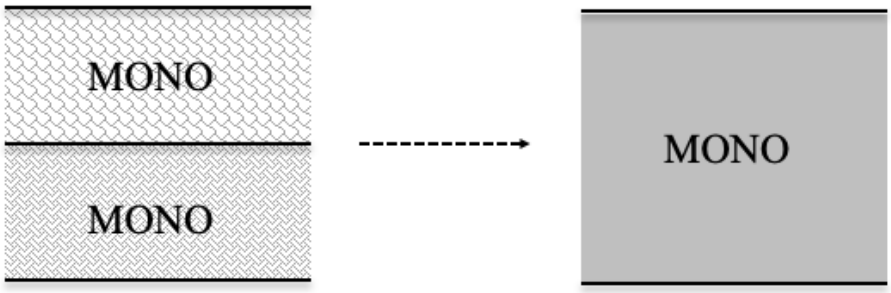

Figure 1: Upscaling schematic diagram of MONO+MONO case.

Table 1: Parameters of periodical MONO+MONO model

Medium	C_{11}	C_{22}	C_{33}	C_{44}	C_{55}	C_{13}	C_{23}
I	15.90	15.50	11.10	2.89	2.34	6.80	5.13
II	9.00	9.84	5.94	2.00	1.60	2.25	2.40
Medium	C_{12}	C_{66}	C_{16}	C_{26}	C_{36}	C_{45}	ρ (gcm^{-3})
I	4.68	2.28	1.10	1.90	2.80	0.50	2.319
II	3.60	2.18	0.90	1.20	2.20	0.80	2.439

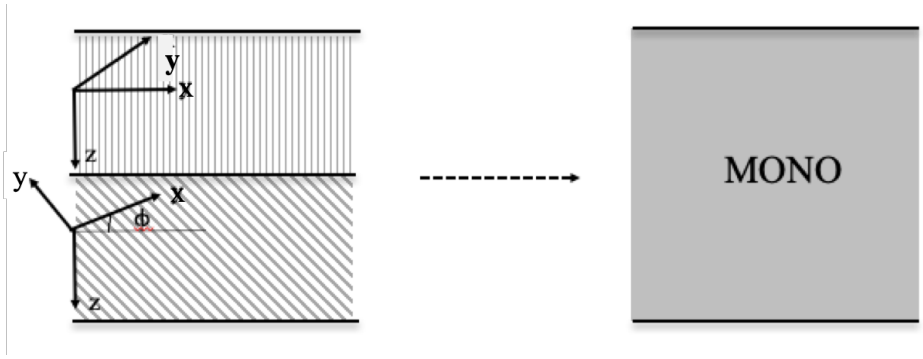

Figure 2: Upscaling schematic diagram of ORT+ORTϕ case.

Since the parameters of rotated ORT medium are defined with ϕ, a table showing the parameter values can not be presented. However, the parameters of normal ORT medium and the definitions of parameters in rotated ORT medium are shown in Appendix B.

A.2 Effective ORT medium

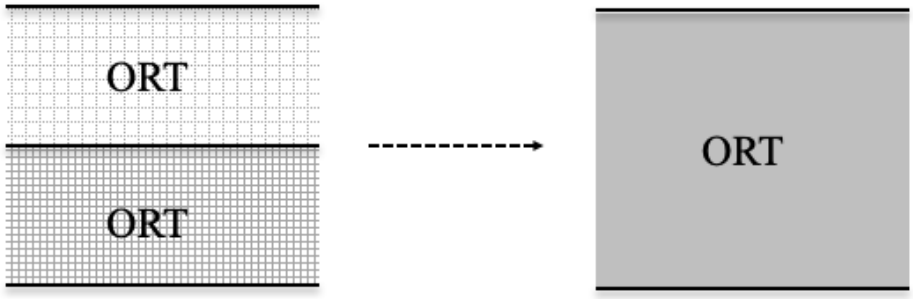

Figure 3: Upscaling schematic diagram of ORT+ORT case.

Table 2: Parameters of periodical ORT+ORT Model

Medium	C_{11}	C_{22}	C_{33}	C_{12}	C_{23}	C_{44}	C_{55}	C_{13}	C_{66}	$\rho\,(\mathrm{gcm}^{-3})$
I	15.90	15.50	11.10	4.68	5.13	2.89	2.34	6.80	2.28	2.319
II	9.00	9.84	5.94	3.60	2.40	2.00	1.60	2.25	2.18	2.439

A.3 Effective VTI medium

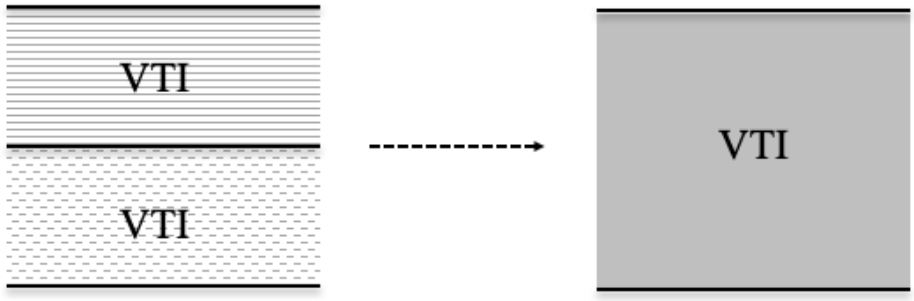

Figure 4: Upscaling schematic diagram of VTI+VTI case.

Table 3: Parameters of periodical VTI+VTI Model

Medium	C_{11}	C_{33}	C_{44}	C_{13}	C_{66}	$\rho\,(\mathrm{gcm}^{-3})$
I	16.91	12.17	4.17	3.66	5.43	2.319
II	32.73	27.43	6.08	17.75	7.46	2.439

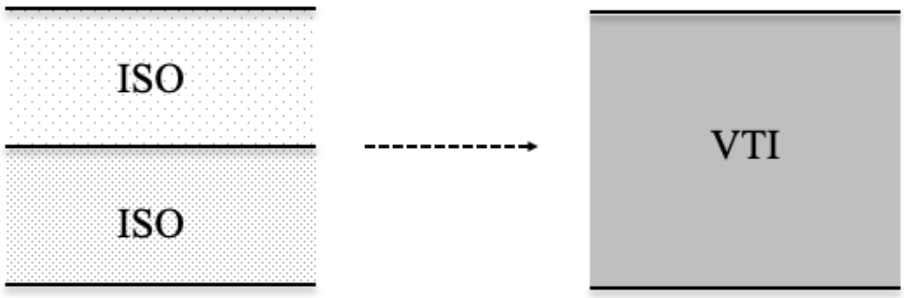

Figure 5: Upscaling schematic diagram of ISO+ISO case

Table 4: Parameters of periodical ISO+ISO Model

Medium	C_{11}	C_{33}	C_{44}	C_{13}	C_{66}	$\rho\,(\mathrm{gcm}^{-3})$
I	12.17	12.17	4.17	3.83	4.17	2.319
II	27.43	27.43	6.08	15.27	6.08	2.439

Appendix B: Azimuthally rotated ORT medium

Model parameters of the original ORT medium without rotation in case ORT+ORTϕ are shown in the table below:

Table 5: Parameters of periodical ORT+ORTϕ model

Medium	C_{11}	C_{22}	C_{33}	C_{44}	C_{55}	C_{13}	C_{23}
I	15.90	15.50	11.10	2.89	2.34	6.80	5.13
Medium	C_{12}	C_{66}	C_{16}	C_{26}	C_{36}	C_{45}	$\rho\,(\mathrm{gcm}^{-3})$
I	4.68	2.28	0.00	0.00	0.00	0.00	2.439

The definitions of parameters in azimuthally rotated ORT medium are shown in Eq. 1

$$
\begin{aligned}
\rho_2 &= \rho_1 \\
C_{332} &= C_{331} \\
C_{362} &= -(C_{131} - C_{231})cos[\phi]sin[\phi] \\
C_{442} &= C_{441}cos[\phi]^2 + C_{551}sin[\phi]^2 \\
C_{452} &= (C_{441} - C_{551})cos[\phi]sin[\phi] \\
C_{552} &= C_{551}cos[\phi]^2 + C_{441}sin[\phi]^2 \\
C_{232} &= C_{231}cos[\phi]^2 + C_{131}sin[\phi]^2 \\
C_{132} &= C_{131}cos[\phi]^2 + C_{231}sin[\phi]^2 \qquad (1) \\
C_{112} &= C_{111}cos[\phi]^4 + 2C_{121}cos[\phi]^2sin[\phi]^2 + C_{221}sin[\phi]^4 + C_{661}sin[2\phi]^2 \\
C_{122} &= \frac{1}{8}(C_{111} + 6C_{121} + C_{221} - 4C_{661} - (C_{111} - 2C_{121} + C_{221} - 4C_{661})cos[4\phi]) \\
C_{162} &= \frac{1}{4}(C_{111} - C_{221} + (C_{111} - 2C_{121} + C_{221} - 4C_{661})cos[2\phi])sin[2\phi]) \\
C_{222} &= C_{221}cos[\phi]^4 + 2C_{121}cos[\phi]^2sin[\phi]^2 + C_{111}sin[\phi]^4 + C_{661}sin[2\phi]^2 \\
C_{262} &= \frac{1}{4}(-C_{111} + C_{221} + (C_{111} - 2C_{121} + C_{221} - 4C_{661})cos[2\phi])sin[2\phi])
\end{aligned}
$$

$$C_{662} = \frac{1}{4}(4C_{661}cos[2\phi]^2 + (C_{111} - 2C_{121} + C_{221})sin[2\phi]^2)$$

where $\rho_{1,2}$ represent the density of medium 1 (original ORT medium) and medium 2 (rotated ORT medium), respectively. $C_{ij1,ij2}$ meansthe elatstic parameters of medium 1 and medium 2, respectively. ϕ is the azimuthal angle with respect to x-direction.

Appendix C: Computational code

C.1 Matlab code

Data manipulating, quality control and upscaling process are done using Matlab R2018b. The codes are shown as following:

```
%%%%%%%backus averaging function
function [vp0, vs0,eps, delta, gamma,ra1,c11a,c13a,c33a,
    c44a,c66a] = average(Data, i, j)

c33 = Data(:,3).^2 .*Data(:,5);
c44 = Data(:,4).^2 .*Data(:,5);
c11 = 2*Data(:,6).*c33 + c33;
c13 = (2*Data(:,7).*c33.*(c33-c44) + (c33-c44).^2).^(0.5) -
     c44;
c66 = 2*Data(:,8).*c44 + c44;

A1=1./c33;
A2=c13./c33;
A3=1./c44;
A4=c11-c13.^2./c33;
A5=c66;

A1a1 = nanmean(A1(i:j));
A2a1 = nanmean(A2(i:j));
A3a1 = nanmean(A3(i:j));
A4a1 = nanmean(A4(i:j));
A5a1 = nanmean(A5(i:j));
ra1=nanmean(Data((i:j),5));

c33a=1/A1a1;
c44a=1/A3a1;
c13a=A2a1/A1a1;
c11a=(A2a1^2+A1a1*A4a1)/A1a1;
c66a=A5a1;
```

```
28
29 vp0 = (c33a/ra1)^(0.5);
30 vs0 = (c44a/ra1)^(0.5);
31 eps = (c11a-c33a)/(2*c33a);
32 delta = ((c13a + c44a)^2 - (c33a-c44a)^2)/(2*c33a*(c33a-
       c44a));
33 gamma = (c66a-c44a)/(2*c44a);
34 end

1  clear;
2  %%%%importing the file
3  filename = '/Users/HP/Documents/MATLAB/Data5.TXT';
4  delimiter = ' ';
5
6  formatSpec = '%f%f%f%f%f%f%f%f%[^\n\r]';
7
8  fileID = fopen(filename,'r');
9
10 dataArray = textscan(fileID, formatSpec, 'Delimiter',
       delimiter, 'MultipleDelimsAsOne', true, 'TextType', '
       string', 'EmptyValue', NaN, 'ReturnOnError', false);
11
12 fclose(fileID);
13 Data5 = [dataArray{1:end-1}];
14 clearvars filename delimiter formatSpec fileID dataArray
       ans;
15
16 %%%%%%function of replacing "," by "."
17 function     comma2point_overwrite( filespec )
18           file     = memmapfile( filespec, 'writable', true );
19           comma    = uint8(',');
20           point    = uint8('.');
21           file.Data( transpose( file.Data==comma) ) = point;
22       end
23 %%%%%%%%%%manipulating data and quality control
24 y = 0;
25 for i = 2 : (length(Data5(:,1))-1)
26 for j = 2 : 8
27 if (Data5 (i, j) < -100) && (Data5(i+1,j) >-100) && (Data5(
       i-1,j) >-100)
28      Data5(i,j) = (Data5(i+1,j) + Data5(i-1,j))/2
29      y = y+1;
30 end
31 end
32 end
33 x = 0;
```

```
for k = 1:length(Data5(:,1))
    for l = 1:8
        if Data5(k,1) <-100
            Data5(k,1) = NaN;
            x = x+1;
        end
    end
end
while max(Data5(:,6)) > 0.6
for i = 2:(length(Data5(:,1))-1)
    if Data5(i,6) > 0.6
        for j = 6:8
            Data5(i,j) = (Data5(i-1,j)+Data5(i+1,j))/2;
        end
    end
end
end

for i = 3:(length(Data5(:,1))-2)
        if Data5(i,3) > 4500 && Data5(i-1,3) < 4500 &&
            Data5(i+1,3) <4500
            Data5(i,3) = (Data5(i+1,3) + Data5(i-1,3))/2;
        elseif Data5(i,3) > 4500
                Data5(i,3) = NaN;
        end
        if Data5(i,4) > 2500 && Data5(i-1,4) < 2500 &&
            Data5(i+1,4) <2500
            Data5(i,4) = (Data5(i+1,4) + Data5(i-1,4))/2;
        elseif Data5(i,4) >2500
            Data5(i,4) = NaN;
        end
end
%%%%%%%creating blocks and backus averaging
[vp0(1), vs0(1), eps(1), delta(1), gamma(1), r(1),c11a(1),
    c13a(1),c33a(1),c44a(1),c66a(1)] = average(Data5, 1,
    4261);
[vp0(2), vs0(2), eps(2), delta(2), gamma(2), r(2),c11a(2),
    c13a(2),c33a(2),c44a(2),c66a(2)] = average(Data5, 4261,
    5934);
[vp0(3), vs0(3), eps(3), delta(3), gamma(3),r(3),c11a(3),
    c13a(3),c33a(3),c44a(3),c66a(3)] = average(Data5, 5934,
    6997);
[vp0(4), vs0(4), eps(4), delta(4), gamma(4),r(4),c11a(4),
    c13a(4),c33a(4),c44a(4),c66a(4)] = average(Data5, 6997,
    7686);
```

```
[vp0(5), vs0(5), eps(5), delta(5), gamma(5),r(5),c11a(5),
    c13a(5),c33a(5),c44a(5),c66a(5)] = average(Data5, 7686,
    8421);
[vp0(6), vs0(6), eps(6), delta(6), gamma(6),r(6),c11a(6),
    c13a(6),c33a(6),c44a(6),c66a(6)] = average(Data5, 8421,
    9340);
[vp0(7), vs0(7), eps(7), delta(7), gamma(7),r(7),c11a(7),
    c13a(7),c33a(7),c44a(7),c66a(7)] = average(Data5, 9340,
    12165);
z1vp0 = [ones(1,4261)*vp0(1) ones(1,1673)*vp0(2) ones
    (1,1063)*vp0(3) ones(1,689)*vp0(4) ones(1,735)*vp0(5)
    ones(1,919)*vp0(6) ones(1,2825)*vp0(7)];
z1vs0 = [ones(1,4261)*vs0(1) ones(1,1673)*vs0(2) ones
    (1,1063)*vs0(3) ones(1,689)*vs0(4) ones(1,735)*vs0(5)
    ones(1,919)*vs0(6) ones(1,2825)*vs0(7)];
z1eps = [ones(1,4261)*eps(1) ones(1,1673)*eps(2) ones
    (1,1063)*eps(3) ones(1,689)*eps(4) ones(1,735)*eps(5)
    ones(1,919)*eps(6) ones(1,2825)*eps(7)];
z1delta = [ones(1,4261)*delta(1) ones(1,1673)*delta(2) ones
    (1,1063)*delta(3) ones(1,689)*delta(4) ones(1,735)*delta
    (5) ones(1,919)*delta(6) ones(1,2825)*delta(7)];
z1gamma = [ones(1,4261)*gamma(1) ones(1,1673)*gamma(2) ones
    (1,1063)*gamma(3) ones(1,689)*gamma(4) ones(1,735)*gamma
    (5) ones(1,919)*gamma(6) ones(1,2825)*gamma(7)];
z1r = [ones(1,4261)*r(1) ones(1,1673)*r(2) ones(1,1063)*r
    (3) ones(1,689)*r(4) ones(1,735)*r(5) ones(1,919)*r(6)
    ones(1,2825)*r(7)];

%%%%%%%plotting log curves
figure;
subplot(1,7,1);
plot(Data5(:,2),Data5(:,1),'g');
line1 = line([0,200],[1016,1016],'linestyle','-','Color','
    red','LineWidth',1.5);
line([0,200],[1271,1271],'linestyle','-','Color','red','
    LineWidth',1.5);
line([0,200],[1433,1433],'linestyle','-','Color','red','
    LineWidth',1.5);
line([0,200],[1538,1538],'linestyle','-','Color','red','
    LineWidth',1.5);
line([0,200],[1650,1650],'linestyle','-','Color','red','
    LineWidth',1.5);
line([0,200],[1790,1790],'linestyle','-','Color','red','
    LineWidth',1.5);
hold on;
```

```
%grid
ylabel('Depth (m)');
%flip the axes
set(gca,'XAxisLocation','top','YAxisLocation','left','ydir'
    ,'reverse');
grid on
grid minor
%set the Y range
ylim([365,2220]);
title('gamma ray (API)');
subplot(1,7,2);
plot(Data5(:,3),Data5(:,1),'g');
hold on
plot(z1vp0,Data5(:,1),'r','Linewidth', 1.5);
ylim([365,2220]);
set(gca,'XAxisLocation','top','YAxisLocation','left','ydir'
    ,'reverse','yticklabel',[]);
title('Vp0 (m/s)');
grid on
grid minor
subplot(1,7,3);
plot(Data5(:,4),Data5(:,1),'g');
hold on
plot(z1vs0,Data5(:,1),'r','Linewidth', 1.5);
ylim([365,2220]);
grid on
grid minor
set(gca,'XAxisLocation','top','YAxisLocation','left','ydir'
    ,'reverse','yticklabel',[]);
title('Vs0 (m/s)');
subplot(1,7,4);
plot(Data5(:,5),Data5(:,1),'g');
hold on
plot(z1r,Data5(:,1),'r','Linewidth', 1.5);
ylim([365,2220]);
grid on
grid minor
set(gca,'XAxisLocation','top','YAxisLocation','left','ydir'
    ,'reverse','yticklabel',[]);
title('rho (g/cm^3)');
subplot(1,7,5);
plot(Data5(:,6),Data5(:,1),'g');
hold on
plot(z1eps,Data5(:,1),'r','Linewidth', 1.5);
ylim([365,2220]);
```

```
131 xlim([-1,1]);
132 grid on
133 grid minor
134 set(gca,'XAxisLocation','top','YAxisLocation','left','ydir'
        ,'reverse','yticklabel',[]);
135 title('eps');
136 subplot(1,7,6);
137 plot(Data5(:,7),Data5(:,1),'g');
138 hold on
139 plot(z1delta,Data5(:,1),'r','Linewidth', 1.5);
140 ylim([365,2220]);
141 xlim([-0.5,0.5]);
142 grid on
143 grid minor
144 set(gca,'XAxisLocation','top','YAxisLocation','left','ydir'
        ,'reverse','yticklabel',[]);
145 title('delta');
146 subplot(1,7,7);
147 plot(Data5(:,8),Data5(:,1),'g');
148 hold on
149 plot(z1gamma,Data5(:,1),'r','Linewidth', 1.5);
150 ylim([365,2220]);
151 xlim([-1,1]);
152 grid on
153 grid minor
154 set(gca,'XAxisLocation','top','YAxisLocation','left','ydir'
        ,'reverse');
155 title('gamma');
```

C.2 Mathematica code

The construction of the effective orthorhombic (ORT) and fracture simulations are carried out using Wolfram Mathematica 10.0.

Test I: ORT+ORTϕ

```
deltan = 1 / 10; deltav = 1 / 5; deltah = 3 / 11;
c111 = c11b * (1 - deltan);
c121 = c12b * (1 - deltan);
c131 = c13b * (1 - deltan);
c221 = c11b * (1 - deltan * (c12b^2 / c11b^2));
c231 = c13b * (1 - deltan * (c12b / c11b));
c331 = c33b * (1 - deltan * c13b^2 / (c11b * c33b));
c441 = c44b;
c551 = c44b * (1 - deltav);
c661 = c66b * (1 - deltah);

c11b = 29.985;
c13b = 11.406;
c33b = 26.673;
c44b = 7.8921;
c66b = 9.1594;
c12b = 11.6662;

modelORT1 = {c111 → 26.9865, c221 → 29.5311, c331 → 26.2391, c441 → 7.8921,
    c551 → 6.31368, c131 → 10.2654, c231 → 10.9622, c121 → 10.4996,
    c661 → 6.66138, c161 → 0, c261 → 0, c361 → 0, c451 → 0, rho1 → 2.3428};

modelORT2 =
  {c112 -> c111 Cos[ϕ]^4 + 2 c121 Cos[ϕ]^2 Sin[ϕ]^2 + c221 Sin[ϕ]^4 + c661 Sin[2 ϕ]^2,
   c122 -> 1/8 (c111 + 6 c121 + c221 - 4 c661 - (c111 - 2 c121 + c221 - 4 c661) Cos[4 ϕ]),
   c132 -> c131 Cos[ϕ]^2 + c231 Sin[ϕ]^2,
   c162 -> -1/4 (c111 - c221 + (c111 - 2 c121 + c221 - 4 c661) Cos[2 ϕ]) Sin[2 ϕ],
   c222 -> c221 Cos[ϕ]^4 + 2 c121 Cos[ϕ]^2 Sin[ϕ]^2 + c111 Sin[ϕ]^4 + c661 Sin[2 ϕ]^2,
   c232 -> c231 Cos[ϕ]^2 + c131 Sin[ϕ]^2,
   c262 -> 1/4 (-c111 + c221 + (c111 - 2 c121 + c221 - 4 c661) Cos[2 ϕ]) Sin[2 ϕ], c332 ->
    c331, c362 -> -(c131 - c231) Cos[ϕ] Sin[ϕ], c442 -> c441 Cos[ϕ]^2 + c551 Sin[ϕ]^2,
   c452 -> (c441 - c551) Cos[ϕ] Sin[ϕ], c552 -> c551 Cos[ϕ]^2 + c441 Sin[ϕ]^2,
   c662 -> 1/4 (4 c661 Cos[2 ϕ]^2 + (c111 - 2 c121 + c221) Sin[2 ϕ]^2), rho2 → 2.3428};

alfa = 1 / 2;

A1 = (1 - alfa) / c331 + alfa / c332;

A2 = (1 - alfa) c131 / c331 + alfa c132 / c332;

A3 = (1 - alfa) c361 / c331 + alfa c362 / c332;

A4 = (1 - alfa) c231 / c331 + alfa c232 / c332;

A5 = (1 - alfa) c441 / (c441 c551 - c451^2) + alfa c442 / (c442 c552 - c452^2);

A6 = (1 - alfa) c551 / (c441 c551 - c451^2) + alfa c552 / (c442 c552 - c452^2);

A7 = (1 - alfa) c451 / (c441 c551 - c451^2) + alfa c452 / (c442 c552 - c452^2);

A8 = (1 - alfa) (c111 - c131^2 / c331) + alfa (c112 - c132^2 / c332);

A9 = (1 - alfa) (c161 - c131 c361 / c331) + alfa (c162 - c132 c362 / c332);
```

```
A10 = (1 - alfa) (c261 - c231 c361 / c331) + alfa (c262 - c232 c362 / c332);

A11 = (1 - alfa) (c661 - c361^2 / c331) + alfa (c662 - c362^2 / c332);

A12 = (1 - alfa) (c221 - c231^2 / c331) + alfa (c222 - c232^2 / c332);

A13 = (1 - alfa) (c121 + c661 - c131 c231 / c331 - c361^2 / c331) +
    alfa (c122 + c662 - c132 c232 / c332 - c362^2 / c332);

rho = (1 - alfa) rho1 + alfa rho2;

c33MONO = 1 / A1;

c11MONO = A8 + A2^2 / A1;

c12MONO = A13 - A11 + A2 A4 / A1;

c13MONO = A2 / A1;

c16MONO = A9 + A2 A3 / A1;

c22MONO = A12 + A4^2 / A1;

c23MONO = A4 / A1;

c26MONO = A10 + A4 A3 / A1;

c36MONO = A3 / A1;

c44MONO = A5 / (A5 A6 - A7^2);

c45MONO = A7 / (A5 A6 - A7^2);

c55MONO = A6 / (A5 A6 - A7^2);

c66MONO = A11 + A3^2 / A1;

vp0 = Sqrt[c33MONO / rho];

vs0 = Sqrt[c55MONO / rho];

eps2 = Simplify[(c11MONO - c33MONO) / 2 / c33MONO];

delta2 =
   ((c13MONO + c55MONO)^2 - (c33MONO - c55MONO)^2) / 2 / (c33MONO - c55MONO) / c33MONO;

gamma2 = (c66MONO - c44MONO) / 2 / c44MONO;

eps1 = Simplify[(c22MONO - c33MONO) / 2 / c33MONO];

delta1 =
   ((c23MONO + c44MONO)^2 - (c33MONO - c44MONO)^2) / 2 / (c33MONO - c44MONO) / c33MONO;

gamma1 = (c66MONO - c55MONO) / 2 / c55MONO;

delta3 =
   ((c12MONO + c66MONO)^2 - (c11MONO - c66MONO)^2) / 2 / (c11MONO - c66MONO) / c11MONO;

ep1 = (c16MONO (c33MONO - c55MONO) - c36MONO (c13MONO + c55MONO)) / c55MONO /
    (c33MONO - c55MONO);

ep2 = (c26MONO (c33MONO - c44MONO) - c36MONO (c23MONO + c44MONO)) / c44MONO /
    (c33MONO - c44MONO);

ep3 = c36MONO / c33MONO;
```

```
ep4 = c45MONO (c44MONO + c55MONO) / (2 c44MONO c55MONO);

Plot[{vp0 /. modelORT1 /. modelORT2 /. ϕ → Pi fi / 180,
   vs0 /. modelORT1 /. modelORT2 /. ϕ → Pi fi / 180},
  {fi, 0, 90}, PlotLegends → {"vp0", "vs0"},
  PlotStyle → {Directive[Red, Thick], Directive[Blue, Thick]}, AxesLabel →
   {Style["ϕ,deg", FontSize → 15], Style["Vp0,Vs0, km/s", FontSize → 15]},
  LabelStyle → Directive[Black, Medium, Bold], ImageSize → 400]

Plot[{eps1 /. modelORT1 /. modelORT2 /. ϕ → Pi fi / 180,
   eps2 /. modelORT1 /. modelORT2 /. ϕ → Pi fi / 180},
  {fi, 0, 90}, PlotLegends → {"ϵ1", "ϵ2"},
  PlotStyle → {Directive[Red, Thick], Directive[Blue, Thick]},
  AxesLabel → {Style["ϕ,deg", FontSize → 15], Style["ϵ1,ϵ2", FontSize → 15]},
  LabelStyle → Directive[Black, Medium, Bold], ImageSize → 400]

Plot[{delta1 /. modelORT1 /. modelORT2 /. ϕ → Pi fi / 180,
   delta2 /. modelORT1 /. modelORT2 /. ϕ → Pi fi / 180,
   delta3 /. modelORT1 /. modelORT2 /. ϕ → Pi fi / 180},
  {fi, 0, 90}, PlotLegends → {"δ1", "δ2", "δ3"}, PlotStyle →
   {Directive[Red, Thick], Directive[Blue, Thick], Directive[Black, Thick]},
  AxesLabel → {Style["ϕ,deg", FontSize → 15], Style["δ1,δ2,δ3", FontSize → 15]},
  LabelStyle → Directive[Black, Medium, Bold], ImageSize → 400]

Plot[{gamma1 /. modelORT1 /. modelORT2 /. ϕ → Pi fi / 180,
   gamma2 /. modelORT1 /. modelORT2 /. ϕ → Pi fi / 180},
  {fi, 0, 90}, PlotLegends → {"γ1", "γ2"},
  PlotStyle → {Directive[Red, Thick], Directive[Blue, Thick]},
  AxesLabel → {Style["ϕ,deg", FontSize → 15], Style["γ1,γ2", FontSize → 15]},
  LabelStyle → Directive[Black, Medium, Bold], ImageSize → 400]

Plot[{ep1 /. modelORT1 /. modelORT2 /. ϕ → Pi fi / 180,
   ep2 /. modelORT1 /. modelORT2 /. ϕ → Pi fi / 180,
   ep3 /. modelORT1 /. modelORT2 /. ϕ → Pi fi / 180,
   ep4 /. modelORT1 /. modelORT2 /. ϕ → Pi fi / 180},
  {fi, 0, 90}, PlotLegends → {"ξ1", "ξ2", "ξ3", "ξ4"},
  PlotStyle → {Directive[Red, Thick], Directive[Blue, Thick],
    Directive[Black, Thick], Directive[Black, Dashed]},
  AxesLabel → {Style["ϕ,deg", FontSize → 15], Style["ξ1,ξ2,ξ3,ξ4", FontSize → 15]},
  LabelStyle → Directive[Black, Medium, Bold], ImageSize → 400]
```

Test II: ORT+ORT (ϕ=90 degrees), the codes for effective elastic parameters and anisotropy parameters need to be modified in order to get the expressions:

```
c33MONO = 1 / A1 /. modelORT2 /. ϕ → Pi / 2;

c11MONO = A8 + A2^2 / A1 /. modelORT2 /. ϕ → Pi / 2;

c12MONO = A13 - A11 + A2 A4 / A1 /. modelORT2 /. ϕ → Pi / 2;

c13MONO = A2 / A1 /. modelORT2 /. ϕ → Pi / 2;

c16MONO = A9 + A2 A3 / A1 /. modelORT2 /. ϕ → Pi / 2;

c22MONO = A12 + A4^2 / A1 /. modelORT2 /. ϕ → Pi / 2;

c23MONO = A4 / A1 /. modelORT2 /. ϕ → Pi / 2;

c26MONO = A10 + A4 A3 / A1;

c36MONO = A3 / A1;

c44MONO = A5 / (A5 A6 - A7^2) /. modelORT2 /. ϕ → Pi / 2 /. c451 → 0;
```

```
c45MONO = A7 / (A5 A6 - A7^2);

c55MONO = A6 / (A5 A6 - A7^2) /. modelORT2 /. ϕ → Pi / 2 /. c451 → 0;

c66MONO = A11 + A3^2 / A1 /. modelORT2 /. ϕ → Pi / 2 /. c361 → 0;

c66MONO /. modelORT2 /. ϕ → Pi / 2 /. c361 → 0;

vp0 = Sqrt[c33MONO / rho];

vs0 = Sqrt[c55MONO / rho] /. c451 → 0;

eps2 = Simplify[(c11MONO - c33MONO) / 2 / c33MONO] /. modelORT2 /. ϕ → Pi / 2;

delta2 = ((c13MONO + c55MONO)^2 - (c33MONO - c55MONO)^2) / 2 / (c33MONO - c55MONO) /
       c33MONO /. modelORT2 /. ϕ → Pi / 2 /. c451 → 0;

gamma2 =
  (c66MONO - c44MONO) / 2 / c44MONO /. c451 → 0 /. c361 → 0 /. modelORT2 /. ϕ → Pi / 2;

eps1 = Simplify[(c22MONO - c33MONO) / 2 / c33MONO] /. modelORT2 /. ϕ → Pi / 2;

delta1 = ((c23MONO + c44MONO)^2 - (c33MONO - c44MONO)^2) / 2 / (c33MONO - c44MONO) /
       c33MONO /. modelORT2 /. ϕ → Pi / 2 /. c451 → 0;

gamma1 = (c66MONO - c55MONO) / 2 / c55MONO;

delta3 = ((c12MONO + c66MONO)^2 - (c11MONO - c66MONO)^2) / 2 / (c11MONO - c66MONO) /
       c11MONO /. modelORT2 /. ϕ → Pi / 2 /. c361 → 0;

ep1 = (c16MONO (c33MONO - c55MONO) - c36MONO (c13MONO + c55MONO)) / c55MONO /
    (c33MONO - c55MONO);

ep1 /. modelORT2 /. ϕ → Pi / 2 /. c451 → 0 /. c361 → 0 /. c161 → 0;

ep2 = (c26MONO (c33MONO - c44MONO) - c36MONO (c23MONO + c44MONO)) / c44MONO /
    (c33MONO - c44MONO);

ep3 = c36MONO / c33MONO;

ep4 = c45MONO (c44MONO + c55MONO) / (2 c44MONO c55MONO);

ep4 /. modelORT2 /. ϕ → Pi / 2 /. c451 → 0 /. c361 → 0 /. c161 → 0;
```

Test III: W=1, ϕ: $\left[-\frac{\pi}{2}, \frac{\pi}{2}\right]$

```
B0 = (1 / Pi) (1 / c33) ∫_-Pi/2^Pi/2 1 dϕ;

B1 = (1 / Pi) (1 / c33) ∫_-Pi/2^Pi/2 (c13 Cos[ϕ]^2 + c23 Sin[ϕ]^2) dϕ;

B2 = (1 / Pi) (1 / c33) ∫_-Pi/2^Pi/2 (- (c13 - c23) Cos[ϕ] Sin[ϕ]) dϕ;

B3 = (1 / Pi) (1 / c33) ∫_-Pi/2^Pi/2 (c23 Cos[ϕ]^2 + c13 Sin[ϕ]^2 ) dϕ;

B4 =
   (1 / Pi) ∫_-Pi/2^Pi/2 ( (c44 Cos[ϕ]^2 + c55 Sin[ϕ]^2) / ( (c44 Cos[ϕ]^2 + c55 Sin[ϕ]^2) (c55 Cos[ϕ]^2 +
         c44 Sin[ϕ]^2) - ( (c44 - c55) Cos[ϕ] Sin[ϕ]) ^2) ) dϕ;

B5 =
   (1 / Pi) ∫_-Pi/2^Pi/2 ( (c55 Cos[ϕ]^2 + c44 Sin[ϕ]^2) / ( (c44 Cos[ϕ]^2 + c55 Sin[ϕ]^2) (c55 Cos[ϕ]^2 +
         c44 Sin[ϕ]^2) - ( (c44 - c55) Cos[ϕ] Sin[ϕ]) ^2)) dϕ;

B6 = (1 / Pi) ∫_-Pi/2^Pi/2 ( ( (c44 - c55) Cos[ϕ] Sin[ϕ]) / ( (c44 Cos[ϕ]^2 + c55 Sin[ϕ]^2)
         (c55 Cos[ϕ]^2 + c44 Sin[ϕ]^2) - ( (c44 - c55) Cos[ϕ] Sin[ϕ]) ^2) ) dϕ;

B7 = (1 / Pi) ∫_-Pi/2^Pi/2 ( (c11 Cos[ϕ]^4 + 2 c12 Cos[ϕ]^2 Sin[ϕ]^2 + c22 Sin[ϕ]^4 + c66 Sin[2 ϕ]^2) -
      (c13 Cos[ϕ]^2 + c23 Sin[ϕ]^2) ^2 / (c33)) dϕ;

B8 = (1 / Pi) ∫_-Pi/2^Pi/2 ( (- 1/4 (c11 - c22 + (c11 - 2 c12 + c22 - 4 c66) Cos[2 ϕ]) Sin[2 ϕ]) -
      (c13 Cos[ϕ]^2 + c23 Sin[ϕ]^2) (- (c13 - c23) Cos[ϕ] Sin[ϕ]) / (c33)) dϕ;

B9 = (1 / Pi) ∫_-Pi/2^Pi/2 ( (1/4 (- c11 + c22 + (c11 - 2 c12 + c22 - 4 c66) Cos[2 ϕ]) Sin[2 ϕ]) -
      (c23 Cos[ϕ]^2 + c13 Sin[ϕ]^2) (- (c13 - c23) Cos[ϕ] Sin[ϕ]) / (c33)) dϕ;

B10 = (1 / Pi) ∫_-Pi/2^Pi/2 ( (1/4 (4 c66 Cos[2 ϕ]^2 + (c11 - 2 c12 + c22) Sin[2 ϕ]^2)) -
      (- (c13 - c23) Cos[ϕ] Sin[ϕ]) ^2 / (c33)) dϕ;

B11 = (1 / Pi)
   ∫_-Pi/2^Pi/2 ( (c22 Cos[ϕ]^4 + 2 c12 Cos[ϕ]^2 Sin[ϕ]^2 + c11 Sin[ϕ]^4 + c66 Sin[2 ϕ]^2) - (c23
         Cos[ϕ]^2 + c13 Sin[ϕ]^2) ^2 / (c33)) dϕ;
```

$$B12 = (1 / Pi) \int_{-Pi/2}^{Pi/2} \left(\left(\frac{1}{8} (c11 + 6\,c12 + c22 - 4\,c66 - (c11 - 2\,c12 + c22 - 4\,c66) \cos[4\phi]) \right) + \left(\frac{1}{4} (4\,c66 \cos[2\phi]^2 + (c11 - 2\,c12 + c22) \sin[2\phi]^2) \right) - (c13 \cos[\phi]^2 + c23 \sin[\phi]^2) (c23 \cos[\phi]^2 + c13 \sin[\phi]^2) / (c33) - (-(c13 - c23) \cos[\phi] \sin[\phi])^2 / (c33) \right) d\phi;$$

Test IV: W=1, ϕ: $[0, \frac{\pi}{2}]$

$$B0 = (2 / Pi) (1 / c33) \int_0^{Pi/2} 1 \, d\phi;$$

$$B1 = (2 / Pi) (1 / c33) \int_0^{Pi/2} (c13 \cos[\phi]^2 + c23 \sin[\phi]^2) \, d\phi;$$

$$B2 = (2 / Pi) (1 / c33) \int_0^{Pi/2} (-(c13 - c23) \cos[\phi] \sin[\phi]) \, d\phi;$$

$$B3 = (2 / Pi) (1 / c33) \int_0^{Pi/2} (c23 \cos[\phi]^2 + c13 \sin[\phi]^2) \, d\phi;$$

$$B4 = (2 / Pi) \int_0^{Pi/2} ((c44 \cos[\phi]^2 + c55 \sin[\phi]^2) / ((c44 \cos[\phi]^2 + c55 \sin[\phi]^2) (c55 \cos[\phi]^2 + c44 \sin[\phi]^2) - ((c44 - c55) \cos[\phi] \sin[\phi])^2)) \, d\phi;$$

$$B5 = (2 / Pi) \int_0^{Pi/2} ((c55 \cos[\phi]^2 + c44 \sin[\phi]^2) / ((c44 \cos[\phi]^2 + c55 \sin[\phi]^2) (c55 \cos[\phi]^2 + c44 \sin[\phi]^2) - ((c44 - c55) \cos[\phi] \sin[\phi])^2)) \, d\phi;$$

$$B6 = (2 / Pi) \int_0^{Pi/2} (((c44 - c55) \cos[\phi] \sin[\phi]) / ((c44 \cos[\phi]^2 + c55 \sin[\phi]^2) (c55 \cos[\phi]^2 + c44 \sin[\phi]^2) - ((c44 - c55) \cos[\phi] \sin[\phi])^2)) \, d\phi;$$

$$B7 = (2 / Pi) \int_0^{Pi/2} ((c11 \cos[\phi]^4 + 2\,c12 \cos[\phi]^2 \sin[\phi]^2 + c22 \sin[\phi]^4 + c66 \sin[2\phi]^2) - (c13 \cos[\phi]^2 + c23 \sin[\phi]^2)^2 / (c33)) \, d\phi;$$

$$B8 = (2 / Pi) \int_0^{Pi/2} \left(\left(-\frac{1}{4} (c11 - c22 + (c11 - 2\,c12 + c22 - 4\,c66) \cos[2\phi]) \sin[2\phi] \right) - (c13 \cos[\phi]^2 + c23 \sin[\phi]^2) (-(c13 - c23) \cos[\phi] \sin[\phi]) / (c33) \right) d\phi;$$

$$B9 = (2 / Pi) \int_0^{Pi/2} \left(\left(\frac{1}{4} (-c11 + c22 + (c11 - 2\,c12 + c22 - 4\,c66) \cos[2\phi]) \sin[2\phi] \right) - (c23 \cos[\phi]^2 + c13 \sin[\phi]^2) (-(c13 - c23) \cos[\phi] \sin[\phi]) / (c33) \right) d\phi;$$

```
B10 =
  (2 / Pi) ∫_0^(Pi/2) ((1/4 (4 c66 Cos[2 ϕ]^2 + (c11 - 2 c12 + c22) Sin[2 ϕ]^2)) -
      (- (c13 - c23) Cos[ϕ] Sin[ϕ]) ^ 2 / (c33)) dϕ;

B11 =
  (2 / Pi) ∫_0^(Pi/2) ((c22 Cos[ϕ]^4 + 2 c12 Cos[ϕ]^2 Sin[ϕ]^2 + c11 Sin[ϕ]^4 + c66 Sin[2 ϕ]^2) - (c23
        Cos[ϕ]^2 + c13 Sin[ϕ]^2) ^ 2 / (c33)) dϕ;

B12 = (2 / Pi) ∫_0^(Pi/2) ((1/8 (c11 + 6 c12 + c22 - 4 c66 - (c11 - 2 c12 + c22 - 4 c66) Cos[4 ϕ])) +
      (1/4 (4 c66 Cos[2 ϕ]^2 + (c11 - 2 c12 + c22) Sin[2 ϕ]^2)) -
      (c13 Cos[ϕ]^2 + c23 Sin[ϕ]^2) (c23 Cos[ϕ]^2 + c13 Sin[ϕ]^2) / (c33) -
      (- (c13 - c23) Cos[ϕ] Sin[ϕ]) ^ 2 / (c33)) dϕ;
```

both two cases share the same following codes

```
c33MONO = 1 / B0;

c11MONO = B7 + B1 ^ 2 / B0;
c12MONO = B12 - B10 + B1 B3 / B0;
c13MONO = B1 / B0;
c16MONO = B8 + B1 B2 / B0;
c22MONO = B11 + B3 ^ 2 / B0;
c23MONO = B3 / B0;
c26MONO = B9 + B3 B2 / B0;
c36MONO = B2 / B0;
c44MONO = B4 / (B4 B5 - B6 ^ 2);
c45MONO = B6 / (B4 B5 - B6 ^ 2);
c55MONO = B5 / (B4 B5 - B6 ^ 2);
c66MONO = B10 + B2 ^ 2 / B0;

vs0 = Sqrt[c55MONO / rho1];

eps2 = Simplify[(c11MONO - c33MONO) / 2 / c33MONO];

delta2 =
  ((c13MONO + c55MONO) ^ 2 - (c33MONO - c55MONO) ^ 2) / 2 / (c33MONO - c55MONO) / c33MONO;

gamma2 = (c66MONO - c44MONO) / 2 / c44MONO;

eps1 = Simplify[(c22MONO - c33MONO) / 2 / c33MONO];

delta1 =
  ((c23MONO + c44MONO) ^ 2 - (c33MONO - c44MONO) ^ 2) / 2 / (c33MONO - c44MONO) / c33MONO;

gamma1 = (c66MONO - c55MONO) / 2 / c55MONO;

delta3 =
  ((c12MONO + c66MONO) ^ 2 - (c11MONO - c66MONO) ^ 2) / 2 / (c11MONO - c66MONO) / c11MONO;

ep1 = (c16MONO (c33MONO - c55MONO) - c36MONO (c13MONO + c55MONO)) / c55MONO /
    (c33MONO - c55MONO);

ep2 = (c26MONO (c33MONO - c44MONO) - c36MONO (c23MONO + c44MONO)) / c44MONO /
    (c33MONO - c44MONO);
```

```
ep3 = c36MONO / c33MONO;
ep4 = c45MONO (c44MONO + c55MONO) / (2 c44MONO c55MONO);
```

Test V: weight function is set to be Gaussian distribution. ϕ: [0, $\frac{\pi}{2}$]

```
model1 = {beta1 -> 100, alfa1 -> 180^2 / (500 Pi^2),
    alfa2 -> 180^2 / (150 Pi^2), beta2 -> 50, ϕ01 -> 0, ϕ02 → Pi / 4};

model2 = {beta1 → 50, alfa1 -> 180^2 / (150 Pi^2),
    alfa2 -> 180^2 / (500 Pi^2), beta2 → 100, ϕ01 -> 0, ϕ02 → Pi / 4};

model3 = {beta1 → 80, alfa1 -> 180^2 / (500 Pi^2),
    alfa2 -> 180^2 / (150 Pi^2), beta2 → 80, ϕ01 -> 0, ϕ02 → Pi / 3};

model4 = {beta1 → 100, alfa1 -> 180^2 / (50 Pi^2),
    alfa2 -> 180^2 / (15 Pi^2), beta2 → 100, ϕ01 -> 0, ϕ02 → Pi / 6};

W = beta1 Exp[-alfa1 (ϕ - ϕ01)^2] + beta2 Exp[-alfa2 (ϕ - ϕ02)^2];

Plot[{W1 /. ϕ → Pi fi / 180, W2 /. ϕ → Pi fi / 180, W3 /. ϕ → Pi fi / 180,
  W4 /. ϕ → Pi fi / 180}, {fi, 0, 90}, PlotLegends → {"W1", "W2", "W3", "W4"},
 PlotStyle → {Directive[Red, Thick], Directive[Blue, Thick],
   Directive[Black, Thick], Directive[Dashed, Thick]},
 AxesLabel → {Style["ϕ,deg", FontSize → 15], Style["W", FontSize → 15]},
 LabelStyle → Directive[Black, Medium, Bold], ImageSize → 400]

c11 = 26.9865; c12 = 10.4996; c13 = 10.2654; c22 = 29.5311;
c23 = 10.9622; c33 = 26.2391; c44 = 7.8921; c55 = 6.31368; c66 = 6.66138;
```

substitute each weight function (W1, W2,W3, W4) seperately into the following codes

$$B0 = \left((1/c33)\int_0^{Pi/2} W\,d\phi\right) \Big/ \int_0^{Pi/2} W\,d\phi;$$

$$B1 = \left((1/c33)\int_0^{Pi/2} W2\left(c13\,Cos[\phi]^2 + c23\,Sin[\phi]^2\right)d\phi\right) \Big/ \int_0^{Pi/2} W2\,d\phi;$$

$$B2 = \left((1/c33)\int_0^{Pi/2} W2\,(-(c13-c23)\,Cos[\phi]\,Sin[\phi])\,d\phi\right) \Big/ \int_0^{Pi/2} W2\,d\phi;$$

$$B3 = \left((1/c33)\int_0^{Pi/2} W2\left(c23\,Cos[\phi]^2 + c13\,Sin[\phi]^2\right)d\phi\right) \Big/ \int_0^{Pi/2} W2\,d\phi;$$

$$B4 = \left(\int_0^{Pi/2} W2\left(\left(c44\,Cos[\phi]^2 + c55\,Sin[\phi]^2\right) / \left(\left(c44\,Cos[\phi]^2 + c55\,Sin[\phi]^2\right)\left(c55\,Cos[\phi]^2 + c44\,Sin[\phi]^2\right) - ((c44-c55)\,Cos[\phi]\,Sin[\phi])^2\right)\right)d\phi\right) \Big/ \int_0^{Pi/2} W2\,d\phi;$$

$$B5 = \left(\int_0^{Pi/2} W2\left(\left(c55\,Cos[\phi]^2 + c44\,Sin[\phi]^2\right) / \left(\left(c44\,Cos[\phi]^2 + c55\,Sin[\phi]^2\right)\left(c55\,Cos[\phi]^2 + c44\,Sin[\phi]^2\right) - ((c44-c55)\,Cos[\phi]\,Sin[\phi])^2\right)\right)d\phi\right) \Big/ \int_0^{Pi/2} W2\,d\phi;$$

$$B6 = \left(\int_0^{Pi/2} W\left(((c44-c55)\,Cos[\phi]\,Sin[\phi]) / \left(\left(c44\,Cos[\phi]^2 + c55\,Sin[\phi]^2\right)\left(c55\,Cos[\phi]^2 + c44\,Sin[\phi]^2\right) - ((c44-c55)\,Cos[\phi]\,Sin[\phi])^2\right)\right)d\phi\right) \Big/ \int_0^{Pi/2} W\,d\phi;$$

```
B7 = (∫_0^Pi/2 W ((c11 Cos[ϕ]^4 + 2 c12 Cos[ϕ]^2 Sin[ϕ]^2 + c22 Sin[ϕ]^4 + c66 Sin[2 ϕ]^2) -
        (c13 Cos[ϕ]^2 + c23 Sin[ϕ]^2) ^ 2 / (c33)) dϕ) / ∫_0^Pi/2 W dϕ;

B8 =
  (∫_0^Pi/2 W ((-1/4 (c11 - c22 + (c11 - 2 c12 + c22 - 4 c66) Cos[2 ϕ]) Sin[2 ϕ]) - (c13 Cos[ϕ]^2 +
        c23 Sin[ϕ]^2) (-(c13 - c23) Cos[ϕ] Sin[ϕ]) / (c33)) dϕ) / ∫_0^Pi/2 W dϕ;

B9 =
  (∫_0^Pi/2 W ((1/4 (-c11 + c22 + (c11 - 2 c12 + c22 - 4 c66) Cos[2 ϕ]) Sin[2 ϕ]) - (c23 Cos[ϕ]^2 +
        c13 Sin[ϕ]^2) (-(c13 - c23) Cos[ϕ] Sin[ϕ]) / (c33)) dϕ) / ∫_0^Pi/2 W dϕ;

B10 =
  (∫_0^Pi/2 W ((1/4 (4 c66 Cos[2 ϕ]^2 + (c11 - 2 c12 + c22) Sin[2 ϕ]^2)) -
        (-(c13 - c23) Cos[ϕ] Sin[ϕ]) ^ 2 / (c33)) dϕ) / ∫_0^Pi/2 W dϕ;

B11 = (∫_0^Pi/2 W ((c22 Cos[ϕ]^4 + 2 c12 Cos[ϕ]^2 Sin[ϕ]^2 + c11 Sin[ϕ]^4 + c66 Sin[2 ϕ]^2) - (c23
        Cos[ϕ]^2 + c13 Sin[ϕ]^2) ^ 2 / (c33)) dϕ) / ∫_0^Pi/2 W dϕ;

B12 = (∫_0^Pi/2 W ((1/8 (c11 + 6 c12 + c22 - 4 c66 - (c11 - 2 c12 + c22 - 4 c66) Cos[4 ϕ])) +
        (1/4 (4 c66 Cos[2 ϕ]^2 + (c11 - 2 c12 + c22) Sin[2 ϕ]^2)) -
        (c13 Cos[ϕ]^2 + c23 Sin[ϕ]^2) (c23 Cos[ϕ]^2 + c13 Sin[ϕ]^2) / (c33) -
        (-(c13 - c23) Cos[ϕ] Sin[ϕ]) ^ 2 / (c33)) dϕ) / ∫_0^Pi/2 W dϕ;

c33MONO = 1 / B0;
c11MONO = B7 + B1 ^ 2 / B0;
c12MONO = B12 - B10 + B1 B3 / B0;
c13MONO = B1 / B0;
c16MONO = B8 + B1 B2 / B0;
c22MONO = B11 + B3 ^ 2 / B0;
c23MONO = B3 / B0;
c26MONO = B9 + B3 B2 / B0;
c36MONO = B2 / B0;
c44MONO = B4 / (B4 B5 - B6 ^ 2);
c45MONO = B6 / (B4 B5 - B6 ^ 2);
c55MONO = B5 / (B4 B5 - B6 ^ 2);
c66MONO = B10 + B2 ^ 2 / B0;

eps2 = Simplify[(c11MONO - c33MONO) / 2 / c33MONO];
```

```
delta2 =
   ((c13MONO + c55MONO) ^ 2 - (c33MONO - c55MONO) ^ 2) / 2 / (c33MONO - c55MONO) / c33MONO;

gamma2 = (c66MONO - c44MONO) / 2 / c44MONO;

eps1 = Simplify[(c22MONO - c33MONO) / 2 / c33MONO];

delta1 =
   ((c23MONO + c44MONO) ^ 2 - (c33MONO - c44MONO) ^ 2) / 2 / (c33MONO - c44MONO) / c33MONO;

gamma1 = (c66MONO - c55MONO) / 2 / c55MONO;

delta3 =
   ((c12MONO + c66MONO) ^ 2 - (c11MONO - c66MONO) ^ 2) / 2 / (c11MONO - c66MONO) / c11MONO;

ep1 = (c16MONO (c33MONO - c55MONO) - c36MONO (c13MONO + c55MONO)) / c55MONO /
    (c33MONO - c55MONO);

ep2 = (c26MONO (c33MONO - c44MONO) - c36MONO (c23MONO + c44MONO)) / c44MONO /
    (c33MONO - c44MONO);

ep3 = c36MONO / c33MONO;

ep4 = c45MONO (c44MONO + c55MONO) / (2 c44MONO c55MONO);
```